HHS Public Access

Author manuscript

Cell Rep. Author manuscript; available in PMC 2022 July 16.

Published in final edited form as:

Cell Rep. 2021 October 26; 37(4): 109877. doi:10.1016/j.celrep.2021.109877.

Conserved heterodimeric GTPase Rbg1/Tma46 promotes efficient translation in eukaryotic cells

Fuxing Zeng[1,2], **Xin Li**[2], **Melissa Pires-Alves**[1], **Xin Chen**[3], **Christopher W. Hawk**[1], **Hong Jin**[1,3,4,5,*]

[1]Department of Biochemistry, University of Illinois at Urbana-Champaign, 600 S. Mathews Avenue, Urbana, IL 61801, USA

[2]Department of Biology, School of Life Sciences, Southern University of Science and Technology, No. 1088 Xueyuan Blvd., Shenzhen 518055, People's Republic of China

[3]Center for Biophysics and Quantitative Biology, University of Illinois at Urbana-Champaign, 600 S. Mathews Avenue, Urbana, IL 61801, USA

[4]Carl R. Woese Institute for Genomic Biology, 1206 West Gregory Drive, University of Illinois at Urbana-Champaign, 600 S. Mathews Avenue, Urbana, IL 61801, USA

[5]Lead contact

SUMMARY

Conserved developmentally regulated guanosine triphosphate (GTP)-binding proteins (Drgs) and their binding partner Drg family regulatory proteins (Dfrps) are important for embryonic development, cellular growth control, differentiation, and proliferation. Here, we report that the yeast Drg1/Dfrp1 ortholog Rbg1/Tma46 facilitates translational initiation, elongation, and termination by suppressing prolonged ribosome pausing. Consistent with the genome-wide observations, deletion of Rbg1 exacerbates the growth defect resulting from translation stalling, and Rbg1 stabilizesmRNAs against no-go decay. Furthermore, we provide a cryoelectron microscopy (cryo-EM) structure of the 80S ribosome bound with Rbg1/Tma46 that reveals the molecular interactions responsible for Rbg1/Tma46 function. The Rbg1 subunit binds to the GTPase association center of the ribosome and the A-tRNA, and the N-terminal zinc finger domain of the Tma46 subunit binds to the 40S, establishing an interaction critical for the

*Correspondence: hjin@illinois.edu.

AUTHOR CONTRIBUTIONS

H.J. and F.Z. designed the study. F.Z., X.L., M.P.-A., and C.W.H. performed the experiments. F.Z. analyzed the data, and X.C. helped on the 5P-Seq data analysis. F.Z. and C.W.H. helped with manuscript preparation. H.J. wrote the paper. All authors discussed the final manuscript.

DECLARATION OF INTERESTS

The authors declare no competing interests

INCLUSION AND DIVERSITY

One or more of the authors of this paper self-identifies as an underrepresented ethnic minority in science. One or more of the authors of this paper self-identifies as living with a disability.

SUPPORTING CITATIONS

The following references appear in the supplemental information: Huang et al.(2009).

SUPPLEMENTAL INFORMATION

Supplemental information can be found online at https://doi.org/10.1016/j.celrep.2021.109877.

ribosomal association. Our results answer the fundamental question of how a paused ribosome resumes translation and show that Drg1/Dfrp1 play a critical role in ensuring orderly translation.

In brief

Conserved heterodimeric GTPase Drg/Dfrp proteins bind to the ribosome, but their function in translation is poorly understood. Zeng et al. find that the yeast homolog of Drg1/Dfrp1, named Rbg1/Tma46, suppresses prolonged ribosomal pausing and promotes efficient translation. The structure of the Rbg1/Tma46-bound ribosome reveals molecular interactions important for their function.

Graphical abstract

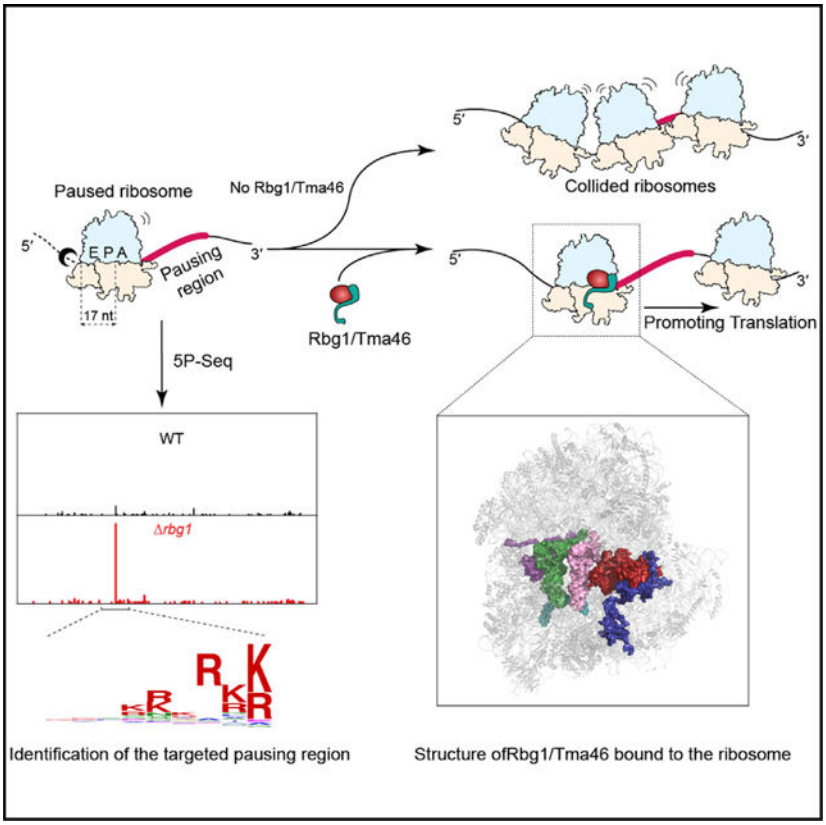

INTRODUCTION

Maintaining protein homeostasis is essential for cell physiology, and this process, undoubtedly, is closely related to the accuracy and efficiency of protein synthesis. Disruption of intracellular homeostasis underlies a wide range of human diseases (Balchin et al., 2016; Labbadia and Morimoto, 2015; Wolff et al., 2014). The central translation apparatus, the ribosome, is a major target of control through its interactions with diverse proteins (Brandman and Hegde, 2016; D'Orazio and Green, 2021; Joazeiro, 2019). One of these proteins, the conserved developmentally regulated guanosine triphosphate (GTP)-binding protein (Drg), plays important roles in embryonic development, cellular growth,

differentiation, and proliferation. Drg was originally identified to be highly expressed in neural precursor cells in the developing mouse brain (Kumar et al., 1992). Shortly after its discovery, Drg mRNA and proteins were found to be widely expressed at variable levels in cultured cells, as well as in other embryonic, postnatal, and adult murine tissues (Sazuka et al., 1992a). The coding sequence of Drg proteins contains a G-motif common to the GTPase superfamily (Leipe et al., 2002; Sazuka et al., 1992b). A phylogenetic study revealed that eukaryotes typically contain two Drg genes, namely, Drg1 and Drg2, that have highly homologous amino acid sequences (Figure S1), whereas archaea contain only one (Li and Trueb, 2000).

In the cell, expression of Drg proteins is affected by Drg family regulatory proteins (Dfrps) through direct physical associations; Dfrp1 specifically binds Drg1, whereas Dfrp2 binds to Drg2 preferentially (Ishikawa et al., 2005). Like the Drgs, the sequences of Dfrp proteins are highly conserved. Yeast and mammalian Dfrp proteins share a partially conserved sequence of about 60 amino acids, the DFRP domain, which is critical for binding to Drg proteins (Figure S1). Importantly, the association of Dfrp and Drg proteins confers stability to the Drg protein *in vivo* (Ishikawa et al., 2005) and enhances the GTPase activity of the Drg *in vitro* (Francis et al., 2012; O'Connell et al., 2009).

Both Drg and Dfrp proteins are conserved from yeast to humans, suggesting that they play important functions in fundamental pathways in eukaryotic cells. These proteins are highly expressed in actively growing and developing cells, as well as adult reproductive tissues of plants, animals, and humans. Consistent with their functions in growth control, altered Drg expression leads to cell transformation or cell cycle arrest (Mahajan et al., 1996; Schenker et al., 1994; Song et al., 2004; Zhao and Aplan, 1998). Although high levels of Drg expression are positively correlated with their functions in translation, and both Drg1/Dfrp1 and Drg2/Dfrp2 complexes copurify with translation factors (Daugeron et al., 2011), the role played by these proteins in translation is not understood. Here, we report molecular functions of the yeast Drg1/Dfrp1 ortholog Rbg1/Tma46 in translation and the structural basis of the mechanism of action on the ribosome.

RESULTS

To effectively study and compare *in vivo* ribosome dynamics in a drug-free way at a genome-wide scale, we used the 5′ monophosphate sequencing (5P-Seq) method (Figures S2A and 2B), which captures 5P mRNA intermediates, produced by 5′ exonucleases (Xrn1 in yeast), that follow the last translating ribosome on an mRNA (Pelechano et al., 2015). As a result, 5P-Seq enriches ribosome footprints on the mRNA undergoing 5′-to-3′ co-translational degradation, providing a sensitive measurement of ribosome dynamics in translation and quality-control pathways. Using this technique, we observe a large degree of ribosome pauses on mRNAs, even in the wild-type (WT) cell, indicating that translation pausing is ubiquitous in the cell.

In parallel, we created the Δ*rbg1* strain and multiple knockouts of genes functionally related to Rbg1. The obviously reduced fitness of yeast cells as a result of double mutants of the Drg/Dfrp family members (Rbg1, Rbg2, Tma46, and Gir2) (Decourty et al., 2008)

suggests at least a partially overlapping functional consequence between the two Drg/Dfrp complexes. Furthermore, yeast genetic screens followed by biochemical investigations showed that one of either the Rbg1/Tma46 or Rbg2/Gir2 complexes was required for uncompromised growth of cells lacking the slh1 gene (Daugeron et al., 2011). The protein product of this gene, Slh1, is another highly conserved eukaryotic protein that associates with ribosomes (Daugeron et al., 2011), and it is known to be important for ribosome-associated quality control (RQC) (D'Orazio et al., 2019; Ikeuchi et al., 2019; Matsuo et al., 2017; Sitron et al., 2017; Sugiyama et al., 2019). Simultaneous functional inactivation of Rbg1, Rbg2, and Slh1 results in serious growth defects (Daugeron et al., 2011). Therefore, we created a conditional triple-knockout strain, Δ*rbg2*Δ*slh1*-Rbg1d, by simultaneously inhibiting Rbg1 mRNA transcription and promoting Rbg1 protein degradation (Nishimura and Kanemaki, 2014; Schuller et al., 2017). This way, when the triple-knockout strain is combined with the single (Δ*rbg1*) and double (Δ*rbg2*Δ*slh1*) knockouts, cellular functions of Rbg1 can be specifically examined and the partially overlapping functions of the three proteins Rbg1, Rbg2, and Slh1 can also be studied (Figure 1A).

Similar growth phenotype patterns were observed at 19°C, 30°C, and 37°C for the WT and all mutant strains (Figure 1B), suggesting that the conditional knockout strain Δ*rbg1*Δ*slh1*-Rbg1d works in the manner expected and that the cellular function of Rbg1 is temperature independent. Furthermore, a progressive decrease in the amount of polysomes and an increase in the amount of 40S, 60S, and 80S ribosomal fractions were observed when cells depleted these three proteins one by one, demonstrating a gradual decrease of global translation as these three proteins are removed from the cell one after another (Figure 1C).

Deletion of Rbg1 leads to accumulation of ribosomes at the start and stop codons

Using the 5P-Seq method, we found that metagene analyses demonstrated progressively increasing peaks at the –14-nucleotide (nt) and 4-nt positions in Δ*rbg1*, Δ*rbg2*Δ*slh1*, and Δ*rbg2*Δ*slh1*-Rbg1d cells (Figure 2A ii–iv, solid lines in blue and red) when compared to the randomly fragmented mRNA control (dotted lines in black) and the WT cells (Figure 2A i). Because the length of ribosomal footprints from the ribosomal P-site to its protected 5′ end is 14 nt in this experiment, these two positions correspond to the ribosome pausing at the start codon and after seven amino acids have entered the exit tunnel, respectively (Figures S3A and 3B).

At the stop codon, we also observe defects of slowed termination in Δ*rbg1* and Δ*rbg2*Δ*slh1*-Rbg1d cells (Figure 2B; Figures S3C and 3D), whereas Δ*rbg2*Δ*slh1* shows only a modest defect, suggesting that, unlike Rbg2 and Slh1 together, Rbg1 alleviates ribosome accumulation at the stop codon. In addition, we found that ribosome pausing at the seventh amino acid was specifically associated with peptides containing a MSxxxxx pattern (Figure S3E; Pelechano et al., 2015). Other than this finding, no consensus sequences at the amino acid or nucleotide levels were found at either the start or stop codons, and no evidence was found that suggests that specific cellular pathways are targeted by this phenomenon (data not shown). These results show that the functions of Rbg1 and Rbg2 are likely not limited to a specialized pathway.

Inactivation of Rbg1, Rbg2, and Slh1 results in redistribution and accumulation of ribosomes in the 5′ end of mRNA

The mRNA degradation machinery closely follows the last translating ribosome in 5P-Seq, for which the translation rate of the last ribosome affects the amount of 5P intermediates and their positions in the coding region of mRNA. As a result, a 3-nt periodicity pattern of the 5P intermediates in the coding region (CDS) informs about ribosome dynamics, for which a strong 3-nt periodicity in the 5′ region of the coding sequence is suggestive of slow translation and weak 3-nt periodicity indicates fast translation (Figure 2C i). It has been suggested that in WT cells it is difficult for the exonuclease to catch up to the last translating ribosome near the start codon because decapping is rate limiting (Pelechano et al., 2015). Compared to those in the WT, Δ*rbg1*, and Δ*rbg2*Δ*slh1* cells, we observe a much clearer 3-nt periodicity pattern of the 5P intermediates in the 5′ end of coding regions in Δ*rbg2*Δ*slh1*-Rbg1d cells (Figures 2A and 2C i), suggesting that the rate of translation elongation was significantly decreased when the cells lost the functions of Rbg1, Rbg2, and Slh1 simultaneously.

To characterize this phenomenon more quantitatively, we calculated the proportion of 5P reads in the ribosome-protected frame for each codon. The proportion score for a control sample, lacking the characteristic 3-nt periodicity pattern, was estimated to be around ~0.33. In agreement with an earlier observation (Pelechano et al., 2015), the proportion scores of 5P reads slowly increase from 0.33 at the start codon to ~0.45 at the 300-nt position in the ribosome-protected frame for the WT cells (Figure 2C ii–iv, black lines). In contrast, the proportion values at the same position of the mRNA increase noticeably faster in the Δ*rbg1* (red line in Figure 2C ii) and Δ*rbg2*Δ*slh1* cells (green line in Figure 2C, iii). However, this value increases to 0.45 immediately after the start codon in the Δ*rbg2*Δ*slh1*-Rbg1d cells (blue line in Figure 2C iv), indicating a substantial decrease in the rate of elongation in these cells.

Rbg1 alleviates ribosome pausing at specific amino acids and mRNA regions

Seemingly stochastic, yet pervasive ribosome pauses were observed at the individual gene level in our data. However, at the metagene level, considering the length of ribosomal footprints from the ribosomal A-, P-, and E-sites to its protected 5′ end are 17 nt, 14 nt, and 11 nt in the 5P-Seq experiment (Figures S3A and S3C), we observed that ribosome pausing is correlated with the translation of glutamic acids, aspartic acids, arginine, and lysine (Figure 3A), as well as tryptophan and glycine, but to a lesser degree.

In agreement with the results at the start and stop codons, no specific cellular pathway is targeted by Rbg1 proteins, which suggests that they play a general role in suppressing translation pause events. Heterogeneity of the peptide sequences is the hallmark of the translation pauses observed in our genomic data. Nevertheless, when we calculated the pause score at each position as described (Guydosh and Green, 2014), with focus on the +/− 10 amino acid regions R/K-rich sequences stood out as one common feature in all Δ*rbg1*, Δ*rbg2*Δ*slh1*, and Δ*rbg2*Δ*slh1*-Rbg1d cells (Figure 3B). This result correlates well with the strong pausing effects of these two amino acids in the ribosome, and an enrichment analysis

was carried out on the most affected R/K-rich mRNA transcripts when Rbg1, Rbg2, and Slh1 are absent (Figure S4).

The conclusions drawn from the genomic investigations described above were tested by comparing the rate at which WT cells grow in the presence of anisomycin to the rate at which cells lacking Rbg1 grow under the same conditions. The antibiotic anisomycin is known to cause translational stalling by binding to the peptidyl transferase center (PTC) of the ribosome (Grollman, 1967). In the presence of 5 and 10 μg/ml of anisomycin, the Rbg1 deletion strain grows observably slower on YEPD plates than WT yeast cells (Figure 4A, the second line of the cell growth), and cells hardly grow when Rbg1, Rbg2, and Slh1 are depleted (Figure 4A, the third line of the cell growth).

To determine if Rbg1 facilitates the translation of mRNA and protects mRNAs harboring stalling signals from degradation that results from mRNA surveillance, we transformed cells with an mRNA construct containing 12 consecutive arginine codons (R_{12}), which is a sequence known to trigger mRNA no-go decay (D'Orazio et al., 2019; Juszkiewicz and Hegde, 2017), and monitored the degree of its translation by using flow cytometry. Based on the experimental design (Figure 4B i), the ratio of GFP/mCherry in counted cell populations is an indicator of the translation of the construct mRNA and the degree of its stability. Compared to the WT cells (Figure 4B ii), deletion of cellular Rbg1 results in a decrease of the median of the GFP/mCherry ratio by over 20% and an increase in the number of cells with low GFP fluorescence (Figure 4B iii and v), indicating an increased degree of mRNA degradation. In contrast, strikingly, the presence of Rbg1 in the Δ*rbg2*Δ*slh1* cells leads to much enhanced GFP fluorescence and GFP/mCherry ratios, compared not only to the Δ*rbg1* cells but also to WT cells for which the NGD factor Slh1 is present (Figure 3B iv and v). This result shows that Rbg1 indeed enhances the translation of the mRNA and protects the RNA from undergoing no-go decay.

Structural basis of enhanced translation by the binding of the heterodimeric GTPase Rbg1/Tma46 to the ribosome

To gain insights into the molecular interactions important for the heterodimeric GTPase function, we obtained a cryoelectron microscopy (cryo-EM) structure of the ribosome with Rbg1/Tma46 bound. A TAP tag was inserted at the end of the yeast chromosomal Rbg1 gene, and the native Rbg1/Tma46 ribosomal complexes were purified from cellular ribosomal fractions by using affinity pull-down. This method allows us to comprehensively sample physiologically relevant functional states of the ribosome when the protein heterodimer binds. A more detailed experimental procedure and the quality of the cryoEM maps are shown in Figures S5A–S5F.

As shown in Figure 5A, we captured ribosomes in the classical ligand binding state, with two tRNAs in the ribosomal A- and P-sites, protein eIF5A (Gutierrez et al., 2013; Pelechano and Alepuz, 2017; Schuller et al., 2017) in the E-site, and Rbg1/Tma46 bound to the GTPase-associated center (GAC). The ribosomes are in the translational state that they assume after peptide bond formation has occurred but before tRNA translocation has taken place, with the nascent peptides attached to the CCA end of the tRNA in the ribosomal A-site.

The HTH (helix-turn-helix) and G-domain of Rbg1 bind to the 60S subunit, with conserved residues in the α4 helix of Rbg1 interacting with the sarcin-ricin loop of the GAC. In this new ribosomal state when Rbg1/Tma46 binds, the G-domain of Rbg1 moves about 26 Å inward toward the A-tRNA and rotates 40 degrees away from the sarcin-ricin loop compared to eEF1A in the guanosine diphosphate (GDP)/Didemnin B-bound state before tRNA accommodation (Figure 5B). Furthermore, compared with the crystal structure of Rbg1/Tma46 (Figure S5G) in isolation, the S5D2L (S5 Domain 2 Like) domain of Rbg1 extends out; charged residues in the loop regions between β6 and β7, as well as α6 and β8, interact with A-tRNA (Figure 5C); and the TGS domain rotates ~17 degrees and binds to h5 of the 18S rRNA (Figure 5D). These interactions are conserved (Figure S6), indicating their functional importance. Earlier studies showed that deletion of the TGS domain in Rbg1, or mutations in Rbg1's G-domain, which compromise either the nucleotide binding or GTPase activities of the protein, failed to rescue the severe growth defect in the triple knockout Δ*rbg1*Δ*rbg2*Δ*slh1* cells (Daugeron et al., 2011).

Tma46 adopts an extended structure and wraps around Rbg1. Their interaction is stabilized by extensive highly conserved hydrophobic contact. The second zinc finger at the N-terminal region of Tma46 is ordered and binds to the gap formed between h16 and h33 of the 40S head and shoulder domains, respectively, establishing an interaction unique to the heterodimeric GTPase that is absent from other known monomeric translational GTPases, such as EF-Tu, EF-G, and RF3 (Figure 5E). This interaction is critical for mediating the ribosomal association of the heterodimeric GTPase. As shown in Figure 5F, deletion of the N-terminal zinc-finger domain of Tma46 completely abolishes binding of Rbg1/Tma46 to the ribosome, regardless of whether Rbg1 is in the GDP- or GTP-bound states. This result demonstrates that the zinc-finger domain of Tma46, although not required for Rbg1/Tma46 heterodimer formation (Francis et al., 2012), is required for ribosomal association.

It came as a pleasant surprise that a general translation factor, eIF5A, was seen in the Rbg1/Tma46-bound ribosomal complex we studied (Figure 5G). This protein is shown to bind to the ribosomal E-site (Melnikov et al., 2016; Schmidt et al., 2016a) and associates with the ribosome when translation stalls (Buschauer et al., 2020; Schmidt et al., 2016b). Translation at proline stretches is facilitated by eIF5A (Gutierrez et al., 2013). Although we indeed observe a strong pause of ribosomes when translating proline in WT cells, deletion of Rbg1 does not exacerbate this effect (data not shown), suggesting the mechanisms by which eIF5A and Rbg1/Tma46 promote translation are related but different.

DISCUSSION

Translation proceeds at a non-uniform rate, and ribosomes pause as they progress down coding sequences on mRNA. As the data demonstrated in this investigation, the ribosome pauses at every codon it encounters to execute the steps of the translation cycle, and that pausing is responsible for the 3-nt periodicity observed in 5P-Seq. The pauses that occur at start and stop codons are longer than those seen in the elongation cycle as the result of the complexity of the events associated with initiation and termination. In the middle of coding sequences, variations in concentrations of cognate tRNAs, as well as elongation factors, play an important role in determining the rates at which particular codons are translated. Besides

the “normal” pause, a prolonged pause of the ribosome could have effects ranging from being an “impediment but inconsequential” to being detrimental, such as a translation arrest due to mRNA secondary structural elements, specific peptide motifs, or damages in the mRNA (Doma and Parker, 2006; Kuroha et al., 2010; Letzring et al., 2010; Vazquez-Laslop et al., 2008; Yan et al., 2019). How ribosomes that have paused for periods beyond the usual during the translation of a particular codon are recognized and targeted, so that protein synthesis can continue, is an important question. In this study, we show that conserved Drg proteins and their partners, Dfrps, play an important role in this process. The genomic experiments reported above show that the yeast ortholog of Drg1/Dfrp1, Rbg1/Tma46, reduces the pausing seen during initiation and termination and enhances the overall rate of elongation. It is possible that the observed initiation arrest and elongation rate decline in all mutant strains, namely, Δ*rbg1*, Δ*rbg2*Δ*slh1*, and Δ*rbg2*Δ*slh1*-Rbg1d, are coupled. Remarkably, these negative impacts are cumulative, with the mildest defect occurring in the single knockout and the most severe defect occurring in the Δ*rbg2*Δ*slh1*-Rbg1d cell. Our subsequent analysis indicates accumulated ribosome pauses underlie the observed phenomenon.

Proposed mechanism of action

Our single-particle cryo-EM reconstruction shows that the Rbg1/Tma46 complex targets translating ribosomes after peptide-bond formation has taken place but before tRNA translocation. How does Rbg1/Tma46 promote efficient translation? In contrast to the altered conformations reported when stalling peptides reside in the exit tunnel without the Rbg1/Tma46 complex (Chandrasekaran et al., 2019; Dimitrova et al., 2009; Wilson and Beckmann, 2011), when Rbg1/Tma46 binds, the ribosomal decoding and PTCs assume conformations similar to what is observed in ribosomes competent to proceed further in the elongation cycle (Figure S7; Ranjan et al., 2021). This result suggests that the Rbg1/Tma46 complex acts by stabilizing pausing ribosomes in a productive conformation. Because Rbg1/Tma46 binds to tRNAs both *in vitro* (Jin Lab, unpublished data) and in the ribosome (this study) and the GTPase binds to the state after peptide-bond formation with the nascent peptide attached to the CCA-end of the A-tRNAs, ribosomal events prior to translocation, such as tRNA binding, accommodation, and peptide transfer, are to be facilitated by Rbg1/Tma46 during protein synthesis (Figure 6).

Compared to ribosome profiling, 5P-Seq highlights the dynamics of ribosomes on mRNAs undergoing co-translational decay. It is worth mentioning that the sheer number of ribosomal pause sites detected by the 5P-Seq experiment, even in the WT cells, and the heterogeneity of the pausing sequences are striking to us, showing that translation pauses are indeed a widespread phenomenon in eukaryotic cells. This phenomenon was also observed in several earlier studies (Davis et al., 2014; Pelechano and Alepuz, 2017; Schuller et al., 2017). Then, how does Rbg1/Tma46 promote efficient translation in such a diverse molecular environment?

Unlike other known monomeric translational GTPases, the heterodimeric GTPase Rbg1/Tma46 binds to the ribosome in both GTP- and GDP-bound states *in vitro* (Figure 5F), indicating that it plays somewhat related, yet distinct functions in translation. It is reasonable

to think that when translation pauses, E-tRNA leaves and vacates the ribosomal E-site. The zinc finger in the Tma46-subunit senses the movements in the 40S and binds to the gap between the head and shoulder domain. Stabilized by the Tma46–40S interaction, nucleotide binding and GTP hydrolysis in the Rbg1-subunit may help the ribosome and tRNAs to navigate through a range of conformational and energetic landscapes resulting from heterogeneous pause signals, thereby achieving an efficient translation. Further investigations are required to demonstrate molecular details in this process. Nevertheless, nucleotide binding and GTP hydrolysis are important for both Rbg1's association with the ribosome and its cellular functions *in vivo* (Daugeron et al., 2011). In addition, Rbg1/Tma46 has relatively low intrinsic nucleotide-binding and GTP-hydrolysis activities, which may help with the replacement of this GTPase by other elongation factors once its task is accomplished in the ribosome.

Because of the conserved nature of Rbg1/Tma46 and the conserved interface between Rbg1/Tma46 and the ribosome, a similar function is likely to be observed in higher eukaryotic organisms. Furthermore, the amino acid sequences of Drg1 and Drg2 are highly homologous with each other. Importantly, residues in Rbg1 that interact with the ribosome and tRNAs are either conserved or highly homologous, not only within the Drg1 family of proteins, but also between Drg1 and Drg2 (Figure S6). This finding indicates that the Drg2 protein likely interacts with translating ribosomes in a similar way.

In contrast, amino acid sequences of Dfrp1 and Dfrp2 are quite different, except for their DFRP domains (Figure S1). This observation indicates that the two Dfrp proteins are involved in different protein-protein interactions to engage Drg proteins to the ribosome, as was also seen in a recent study of colliding yeast ribosomes involving Gcn1 while this work was under peer review (Pochopien et al., 2021). Our structure explains earlier experimental observations that Dfrp1 specifically binds Drg1 and that Dfrp2 binds to Drg2 preferentially (Ishikawa et al., 2005). As seen in the structure, molecular interactions between Rbg1 and Tma46 are largely hydrophobic (Figure S1 and S6). However, Rbg2 does not possess the same hydrophobic amino acids at the protein interface as Rbg1 (Figure S6). This molecular difference explains why Tma46 and Rbg2 do not associate. On the other hand, certain hydrophobic residues in Tma46 are conserved in Gir2, which also contains residues that could potentially interact with Rbg1 by other interactions at the protein interface, for example, by formation of hydrogen bonds. Nevertheless, the weak cross association of Drg1 and Dfrp2 (Wout et al., 2009), in the otherwise specific and distinct complexes, rules out the strict exclusiveness of the two Drg/Dfrp classes and suggests another fine-tuned layer of control in the cell.

Furthermore, although the two Drg proteins likely interact with the ribosome in a similar manner, they are obviously involved in different translational events due to their distinct Dfrp partners. Based on the data from flow cytometry (Figure 4B), in which Rbg1 in the Δ*rbg2*Δ*slh1* cell leads to a stronger GFP signal produced from the translation of mRNA with stalling sequences compared to the WT cells, Drg1 likely plays a more general role than Drg2 in the cell.

Translation pauses can be viewed as a two-sided events; from the point of view of protein synthesis, a pause needs to be suppressed so that protein synthesis can be resumed and the protein can be made efficiently. However, on the other hand, a pause also provides a valuable chance for regulation. Whether Drg1/Dfrp1 acts as a suppressor of ribosome pausing at sites where mistakes can occur is an important question for future study.

Functional interplay of Drg1/Dfrp1, Drg2/Dfrp2, and ASCC3

The cumulative effects observed in this study among Δ*rbg1*, Δ*rbg2*Δ*slh1*, and Δ*rbg2*Δ*slh1*-Rbg1d cells strongly suggest shared functions for Drg/Dfrp and ASCC3 (the mammalian counterpart of Slh1) proteins in fundamental biological processes. Although it is still possible that the direct cellular targets and molecular functions of these proteins are not the same, available evidence shows that the ribosome is one of their shared targets. Here, we propose that these three proteins help to ensure cellular protein homeostasis by targeting ribosomes involved at the junction of protein synthesis and quality-control pathways (Figure 6). When translation pauses, the Drg/Dfrp complex helps ribosomes to navigate through and find their way to pass the pauses, thereby allowing the trailing ribosomes to continue using the mRNA as a template for protein synthesis. In the absence of Drg/Dfrp, ASCC3 likely guides the paused ribosome to the quality-control pathway. Because the exact role of ASCC3 in RQC or NGD is unclear, more investigations will be needed to reveal these details at the molecular level.

Although secondary effects resulting from protein deletion have been minimized in our experiments, the direct relation between Rbg1 protein depletion and altered ribosome dynamics requires biochemical reconstitution. Likewise, *in vitro* biochemical reconstitution combined with genetic manipulation to address functional redundancy will be required to establish a detailed mechanism of Rbg1 in the ribosome. In addition, whether Rbg1/Tma46 participates in RQC is an important question to answer in future investigations.

Drg proteins play important roles in some cellular processes that appear to be unrelated to translation. For example, they are involved in spindle checkpoint signaling, and elevated levels of the Drg1 protein causes lung adenocarcinoma and taxol resistance (Lu et al., 2016). In an *in vitro* study, Drg1 was reported to diffuse on microtubules, to promote microtubule polymerization, and to drive microtubule bundle formation in a GTP-independent manner (Schellhaus et al., 2017). Additionally, HeLa cells with reduced Drg1 levels show delayed progression from prophase to anaphase due to a slowed spindle formation (Schellhaus et al., 2017). Further investigations are required to see if these seemingly unrelated processes crosstalk with translation.

Maintaining protein homeostasis during critical stages and conditions such as development, proliferation, and cellular stress is critical for eukaryotic organisms. It is not surprising that the translational machinery is one of the major targets of regulation for this purpose. Our observations provide the link between translation, ribosome pause, and protein quality control, a critical component for maintaining protein homeostasis and cell physiology. It is worth mentioning that other pathways may crosstalk with these processes to achieve cellular homeostasis.

STAR★METHODS

RESOURCE AVAILABILITY

Lead contact—Further information and requests for resources and reagents should be directed to and will be fulfilled by the lead contact, Hong Jin (hjin@illinois.edu)

Materials availability—All unique/stable reagents generated in this study are available from the lead contact with a completed materials transfer agreement.

Data and code availability

- The sequencing data for 5P-Seq experiment have been deposited in NCBI's Gene Expression Omnibus and are accessible through GEO series accession numbers GSE154212. Electron microscopy maps have been deposited in the Electron Microscopy Data Bank under accession codes EMD-24652. Coordinates have been deposited in the Protein Data Bank under accession code 7RR5. All deposited datasets are publicly available as of the date of publication. This paper used existing, publicly available data: the accession codes of the deposited PDB IDs are listed in the key resources table.
- All original code has been deposited at Figshare and is publicly available as of the date of publication. DOIs are listed in the key resources table.
- Any additional information required to reanalyze the data reported in this paper is available from the lead contact upon request.

EXPERIMENTAL MODEL AND SUBJECT DETAILS

Yeast—Yeast strains used in this study can be found in Table S1. Unless indicated otherwise in the Method details section, yeast cells were grown in YEPD at 30°C in a shaking incubator, or were grown on YEPD+agar plates at 30°C.

Bacteria—*E. coli* BL21(DE3) were used to co-overexpress Rbg1 and Tma46 and were grown in LB medium at 37°C in a shaking incubator. Cell lines used in this study are listed in the Key resources table and Table S1.

METHOD DETAILS

Yeast strains and growth conditions—*Saccharomyces cerevisiae* strains with BY4742 (*MATα his3Δ1 leu2Δ0 lys2D0 ura3Δ0*) background were used in this study. Chromosomal insertion and knockout strains with this background were obtained by established homologous recombination techniques (Baudin et al., 1993; Longtine et al., 1998), and are listed in Table S1. The plasmids used here were constructed via standard cloning strategies and are listed in Table S2. To generate C-terminal, chromosomally TAP-tagged strains, the TAP-*URA3* cassette, contained in the modified p415G plasmid, was amplified with homology regions to replace the stop codon of the gene to be tagged. Strains were confirmed by sequencing across the entire fusion gene, as well as western blot detection of the calmodulin binding peptide (CBP) epitope. It has been reported that cellular growth of the Δ*rbg1*Δ*rbg2*Δ*slh1* strain was severely impaired (Daugeron et al., 2011). To control the

Rbg1 protein level in the cell, a mini auxin-inducible degron (mAID) tag was inserted chromosomally into the Δ*rbg2*Δ*slh1* strain, at the 5′ end of the Rbg1 gene, with a sequence containing the *KanMX*-GAL10p-mAID-Flag epitope before the start codon of Rbg1 (Schuller et al., 2017).

To obtain polysome profiles and perform 5P-Seq experiments, wild-type and mutant cells were grown to an OD_{600} of 0.6 in YPGR (2% galactose + 0.2% raffinose) medium at 30°C, harvested by centrifugation, then washed and resuspended in the same volume of YEPD (2% glucose) medium containing 1 mM auxin (Sigma-Aldrich). These cells were grown in the presence of auxin for another 20 minutes at 30°C to deplete Rbg1 completely.

Plasmids—Genes encoding Rbg1 and Tma46 were amplified from the genomic DNA of *S. cerevisiae* and were cloned into modified pET28a or pET22b vectors using standard cloning strategies. Mutants were generated by mutagenesis PCR using the Q5 Site-Directed Mutagenesis Kit (NEB), according to the manufacturer's instructions.

Purification of ribosomes, proteins—Yeast ribosomes from the YAS2488 strain were purified according to published methods (Acker et al., 2007). Briefly, yeast cells grown to exponential phase were harvested and resuspended in ribosome lysis buffer (20 mM HEPES-KOH, pH 7.4, 100 mM KOAc, pH 7.6, 2.5 mM $Mg(OAc)_2$, 1 mg/ml Heparin, 2 mM DTT, 0.5 mM AEBSF). Cells were frozen in liquid nitrogen and were broken using an RNase-free mortar and pestle. Extracts were clarified at 18,000 × *g* for 10 minutes at 4°C, and then loaded onto 1.1 M sucrose cushions in the cushion buffer (20 mM HEPES-KOH, pH 7.4, 100 mM KOAc, pH 7.6, 2.5 mM $Mg(OAc)_2$, 500 mM KCl, 2 mM DTT). Cushions were centrifuged at 39,000 rpm for 5 hours and 20 minutes in a Beckman Type 45 Ti rotor and the pellets were resuspended in the resuspension buffer (20 mM HEPES-KOH, pH 7.4, 50 mM KCl, 5 mM $Mg(OAc)_2$, 0.1 mM PMSF, 0.1 mM benzamidine, 2 mM DTT) before being loaded onto 10% to 40% sucrose gradients with the same buffer and centrifuged at 32,000 rpm for 5 hours in SW 32.1 Ti rotor. The 80S peaks were collected and buffer exchanged to the reassociation buffer (3 mM HEPES-KOH, pH 7.4, 6.6 mM Tris-HOAc, pH 7.2, 3 mM NH_4Cl, 6.6 mM NH_4OAc, 48 mM KOAc, 4 mM $Mg(OAc)_2$, 2.4 mM DTT). Purified ribosomes were stored at −80°C.

Wild-type and mutant Rbg1 and Tma46 were cloned and co-overexpressed in BL21(DE3) cells, then purified by affinity and ion-exchange chromatography (Francis et al., 2012). Plasmids containing rbg1 and tma46 genes were co-transformed into BL21(DE3). Cells were grown in LB medium at 37°C until an OD_{600} of 0.8 was reached, then protein expression was induced by incubation with 0.3 mM IPTG at 16°C for 18 hours. Cells were harvested, resuspended in Ni-NTA buffer (50 mM Tris, pH 7.5, 200 mM NaCl, 5% glycerol) and disrupted by French Press, followed by centrifugation at 18,000 rpm for 30 minutes. Cell extracts were passed through a Ni-NTA column and were eluted with Ni-NTA buffer supplemented with 200 mM imidazole. After exchanging into the buffer A (50 mM Tris, pH 7.5, 100 mM NaCl, 5% glycerol), proteins were purified by a HiTrap Q HP column (Cytiva). Purified proteins were concentrated and stored at −80°C.

Ribosome binding assay—Purified Rbg1/Tma46 or Rbg1/Tam46-ΔZnF complexes were incubated with GDPCP or GDP for 15 minutes at 30°C in polysome lysis buffer (20 mM Tris-HCl, pH 8.0, 140 mM KCl, 1.5 mM $MgCl_2$, 1% (v/v) Triton X-100, 1 mM DTT, 100 μg/ml cycloheximide) followed by addition of purified 80S for another 30 minutes. The factor-bound ribosomal complexes were then separated by sedimentation through a 10%–50% sucrose gradient in polysome lysis buffer. Binding of Rbg1/Tma46 to the ribosome was determined by western blot. Flag-tagged RPL25 was immunoblotted as control.

Cell growth assay—Cell growth rates were determined by a spot assay as reported (Xu et al., 2014) with minor modifications. Cells were first grown to exponential phase at 30°C in either YPGR or YEPD, depending upon the strain used. Then 0.5 OD_{600} units of cells were pelleted and resuspended in 0.5 mL of 1 × PBS buffer. The following serial dilutions were prepared in 1x PBS buffer: 1/5, 1/25, 1/125, and 1/625, and 1 μl of each dilution was spotted on YEPD agar plates. 1 mM auxin (Sigma-Aldrich) was added for assays of Δ*rbg2*Δ*slh1*-Rbg1d strains. Images were taken after 2 to 5 days of growth at 30°C.

Polysome profiling—Yeast cells were grown at 30°C until they reached an OD_{600} of 0.6, then were treated with 100 μg/ml of cycloheximide for 2 minutes before harvesting. Cells were quickly harvested by centrifugation and were washed twice with ice-cold polysome lysis buffer. The cell pellet was resuspended in 1 mL of polysome lysis buffer supplemented with EDTA-free protease inhibitors (Roche) and was grounded in liquid nitrogen using an RNase-free mortar and pestle. Extracts were clarified at 18,000 × *g* for 10 minutes at 4°C, then loaded onto 10%–50% sucrose gradients in polysome gradient buffer (20 mM Tris-HCl, pH 8.0, 140 mM KCl, 5 mM $MgCl_2$, 20 U/ml SUPERase In (Fisher Scientific), 0.5 mM DTT, 100 μg/ml cycloheximide). Gradients were centrifuged at 32,000 rpm for 3 hours and 45 minutes in a Beckman SW 32.1 Ti rotor and polysome profiles were generated by fractionation with continuous measurement of absorbance at 260 nm.

Western blot—Western blotting was performed as described (Zeng and Jin, 2016). Briefly, Fractions from polysome profiles were resolved via SDS-PAGE, and proteins of interest were transferred to nitrocellulose membranes (GE Healthcare Amersham) for 40 minutes at 100 V in a Mini Trans-Blot apparatus (Bio-Rad). Protein bands were detected with either anti-Flag (Sigma-Aldrich) or anti-His antibodies (Sigma-Aldrich).

5P-Seq library preparation—5P-Seq libraries were prepared as described (Pelechano et al., 2015, 2016). Yeast strains were grown in 50 mL YPGR medium until they reached an OD_{600} of 0.6. Cells were then harvested, and their media exchanged for 50 mL YEPD containing 1 mM auxin (Sigma-Aldrich), followed by an additional 20 minutes of incubation. Cells were harvested quickly by centrifugation. Total RNA was extracted, and DNA was removed by incubation with TURBO DNase (Invitrogen) for 30 minutes at 37°C. For control libraries, 50 μg of DNA-free total RNA was fragmented by incubation at 80°C for 5 minutes in RNA fragmentation buffer (40 mM Tris-acetate, pH 8.1, 100 mM KOAc, 30 mM $Mg(OAc)_2$). Fragmented 5′-OH sites were phosphorylated by treatment with 5 units of T4 polynucleotide kinase (NEB) for 1 hour at 37°C, followed by phenol:chloroform extraction. The phosphorylated 5′ ends were subjected to RNA ligation by 20 units of T4

RNA ligase (Promega) in the presence of 10 mM DNA/RNA rP5_RND oligo (Table S3) at 16°C overnight. For the 5P-Seq libraries, 50 μg of DNA-free total RNA was directly ligated to the rP5_RND oligo in the same conditions as specified for control samples. The polyadenylated mRNAs were enriched using Dynabeads $(dT)_{25}$ (Invitrogen), according to the manufacturer's instructions, followed by fragmentation for 5 minutes at 80°C in RNA fragmentation buffer. Both the controls and 5′ RNA-seq samples were primed with random hexamers and reverse transcribed with Superscript II (Thermo Fisher). Second strand cDNA synthesis was performed using a single PCR cycle (98°C for 1 minute, 50°C for 2 minutes, and 72°C for 15 minutes) in Phusion High-Fidelity PCR Master Mix (NEB) and was primed with BioNotI-P5-PET (Table S3). Double-stranded cDNA was purified using HighPrep beads (Magbio), then was bound to Dynabeads M-280 Streptavidin beads (Invitrogen). Bound DNA molecules were subjected to end repair, adenine addition, and adaptor ligation via addition of 0.5 μL of P7MPX annealed adaptor, which was prepared by annealing the P7MPX_linker_for and P7MPX_linker_rev (Table S3) primers at a final concentration of 2.5 μM. The Dynabead-bound DNA was washed and subjected to PCR amplification (98°C for 30 s; 18 cycles of the following condition: 98°C for 20 s, 65°C for 30 s, 72°C for 30 s; 72°C for 5 minutes) using Phusion High-Fidelity PCR Master Mix with HF buffer (NEB), 0.1 μM of PE1.0, and the appropriate PE2_MPX_01 to PE2_MPX_08 primers (Table S3). Samples were size-selected using 0.6x-0.9x (v/v) HighPrep beads (Magbio), separated via agarose gel electrophoresis, and the 300–500 bp regions of the gel were extracted. Libraries were sequenced using single-end, 100 bp-read NovaSeq Illumina sequencing with 6 nt indexing reads for library identification.

Flow cytometry—Overnight cultured cells carrying the dual fluorescence reporter gene with a stalling sequence containing twelve consecutive arginine codons were first inoculated into 50 mL YEPD with initial OD_{600} = 0.1 and grown to mid-log phase at 30°C. Cells were then collected and diluted to OD_{600} = 0.1 and about 10,000 cells were analyzed with a FACSCanto SORP flow cytometer for GFP and mCherry fluorescence detection using 488 nm and 561 nm excitation lasers, respectively. Data were analyzed by Flow JO software with scatterplots showing the intensity of GFP and mCherry for individual cells. Cells with > 10^3 RFU mCherry intensities were selected and the GFP/mCherry ratios were calculated and shown as violin plots using Origin software. Flow cytometry was done in triplicate.

Electron microscopy, data collection and image processing: *S. cerevisiae* with C-terminally TAP-tagged Rbg1 were grown to log phase at 30°C, then were treated with 100 μg/ml of cycloheximide for 2 minutes before being harvested by centrifugation. The harvested cells were resuspended in one-third volume of polysome lysis buffer and were grounded in liquid nitrogen. Cell extracts were clarified at 20,000 × *g* for 30 minutes at 4°C and incubated with IgG beads for 1 hour at 4°C. The complex-bound beads were washed three times with polysome lysis buffer, and the Rbg1/Tma46 bound ribosomal complexes were eluted by incubation with TEV for 1 hour at 20°C. 0.05% glutaraldehyde was added to the eluted complex and incubated for 30 minutes on ice. The crosslinking reaction was quenched by 25 mM Tris-HCl (pH 7.5) and 0.01% n-do-decyl-D-maltoside (DDM) was added to the final solution. Sample preparation for cryoEM studies was performed as described (Zeng et al., 2017). 2.5 μl aliquots of ribosomal complexes were incubated for 30

s on glow-discharged Holley carbon grids with a thin-layer carbon film cover (Quantifoil). Grids were blotted using a Vitrobot Mark IV (FEI) for 3 s in 100% humidity at 4°C, then were plunge frozen into liquid ethane. Data were collected in vitreous ice using Titan Krios G3i (D3796) transmission electron microscopes operating at 300 keV with FEI Falcon III detectors. A total of 11,529 micrographs were acquired using a dose of 30 $e^{-}Å^{-2}$. The drifts of movie frames were corrected using MotionCor2 (Zheng et al., 2017), and the contrast transfer functions were determined using CTFFIND4 (Rohou and Grigorieff, 2015). Data processing was carried out in Relion3 (Zivanov et al., 2018). A total of 1,222,865 particles were picked and extracted for reference-free 2D classification. 737,448 particles were selected and subjected to 3D refinement program followed by 3D classification with a mask around the ribosome GTPase association center. The class displaying good factor density (95,380 particles) was subjected to 3D refinement to yield a reconstruction at 3.23 Å . Resolutions were reported based upon the gold-standard Fourier shell correlation (FSC) of 0.143 criterion (Scheres and Chen, 2012).

Model building, refinement, and validation—The high-resolution crystal structure of the yeast 80S ribosome (PDB: 4V88) (Ben-Shem et al., 2011) was fit into the EM density map using rigid body fitting in Chimera (Pettersen et al., 2004). The body, head, and shoulder domains of the 40S, L1 stalk and P stalk of the 60S were fit separately using Coot (Emsley et al., 2010). Ribosome-bound ligands, A-tRNA, P-tRNA and eIF5A, were built into the density map in Coot using PDB 5GAK as a reference (Schmidt et al., 2016a). The crystal structure of the Rbg1/Tma46 complex (PDB: 4A9A) (Francis et al., 2012) was used as a reference, and the HTH, S5D2L, G domain, and TGS domain of Rbg1 and each helix of Tma46 were built into the density map accordingly. The second zinc finger of Tma46 was built using the homology model generated by SWISS-MODEL (Waterhouse et al., 2018).

The model obtained was refined using Phenix with secondary structure, RNA base-pair, sugar pucker and base stacking restraints (Liebschner et al., 2019). The final model was validated using MolProbity (Williams et al., 2018). Refinement statistics for the structures were summarized in Table S4. Figures were made in Chimera (Pettersen et al., 2004) and Pymol (Schrodinger, 2015).

QUANTIFICATION AND STATISTICAL ANALYSIS

High throughput sequencing data processing and analysis—For all libraries, reads were first demultiplexed using the index sequences. The 3′ adaptor sequence was identified and removed using the cutadapt package (Martin, 2011). After adaptor removal, the remaining reads were deduplicated by bbmap (BBMap - Bushnell B. -https://sourceforge.net/projects/bbmap/) based upon random barcode sequences, and the 5′ UMI were trimmed by fastx_trimmer (Hannon, 2010, FASTX-Toolkit.). Non-coding RNAs were filtered by mapping to annotated *S. cerevisiae* rRNAs, tRNAs, snRNAs, and snoRNAs using Bowtie1 (Langmead et al., 2009). Unaligned reads were then mapped to the sacCer3 genome using Bowtie2 (Langmead and Salzberg, 2012) with the arguments: '–local -D 15 -R 2 -N 1 -L 20 -i S,1,0.75 -S'.

Unless indicated otherwise, data analysis was performed using a series of custom scripts written in Python. For the 5P-Seq experiment, reads with multiple alignments, mapping quality values < 30, or those containing soft-clipped bases on the 5′ end were excluded from downstream analysis. The 5′ ends of reads passing quality filtering were extracted and the total numbers of reads per genome location were calculated. Reads per million (RPM) values for each genomic locus were calculated using the number of unique reads. Only genes with reads per million per kilobase (RPKM) values of greater than 20 were chosen for further analysis. To create meta gene plots, we calculated the average rpm of the 5′ ends from all biological replicates. These 5′ ends were then aligned relative to the stop codon (or any specific codon) of all ORFs, and the sum of the 5′ends reads was determined at each position. To analyze ribosome pausing around the start codon, genes were sorted by a ratio value which is calculated by dividing the read counts at −14 nt or 4 nt by the total read counts corresponding to the surrounding ± 2 codons, as previously described (Pelechano et al., 2015). Then the first 8 amino acids of the ORF were extracted. Sequences of the top 50% of genes were compared to the bottom 50% using MEME (Bailey et al., 2009). To characterize the elongation pausing, we calculated the pause score, as described previously, with minor modifications (Guydosh and Green, 2014). Pause scores were calculated by dividing the rpm value at each genomic position by the mean of the rpm values in the ± 10-codon region surrounding the position. Regions in the first and last 10 codons of the ORF were excluded. Amino acid sequences with pause scores > 10 were considered to be stalling sites. Stalling sequences were calculated by MEME (Bailey et al., 2009) using the sequences with pause score < 10 as a control.

Supplementary Material

Refer to Web version on PubMed Central for supplementary material.

ACKNOWLEDGMENTS

We thank Prof. Peter Moore at Yale University for critical comments on the manuscript. We also thank the Cryo-EM Center at Southern University of Science and Technology, Junyi Jiang and Qingrong Li in the F. Zeng laboratory, Dr. Bridget Carragher and Dr. Ed Eng at the National Center for CryoEM Access and Training (NCCAT) and Dr. Valerie Tokars at Northwestern University for their help on cryoEM data collection, the core Research Facility at Southern University of Science and Technology for flow cytometry, Roy J. Carver Biotechnology Center at the University of Illinois at Urbana-Champaign for sequencing, and members in the Jin laboratory for helpful discussions. H.J. acknowledges support from the National Institute of General Medical Sciences of the NIH (R01-GM120552).

REFERENCES

Acker MG, Kolitz SE, Mitchell SF, Nanda JS, and Lorsch JR (2007). Reconstitution of yeast translation initiation. Methods Enzymol. 430, 111–145. [PubMed: 17913637]

Bailey TL, Boden M, Buske FA, Frith M, Grant CE, Clementi L, Ren J, Li WW, and Noble WS (2009). MEME SUITE: tools for motif discovery and searching. Nucleic Acids Res. 37, W202–W208. [PubMed: 19458158]

Balchin D, Hayer-Hartl M, and Hartl FU (2016). In vivo aspects of protein folding and quality control. Science 353, aac4354.

Baudin A, Ozier-Kalogeropoulos O, Denouel A, Lacroute F, and Cullin C (1993). A simple and efficient method for direct gene deletion in Saccharomyces cerevisiae. Nucleic Acids Res. 21, 3329–3330. [PubMed: 8341614]

Ben-Shem A, Garreau de Loubresse N, Melnikov S, Jenner L, Yusupova G, and Yusupov M (2011). The structure of the eukaryotic ribosome at 3.0 Å resolution. Science 334, 1524–1529. [PubMed: 22096102]

Brandman O, and Hegde RS (2016). Ribosome-associated protein quality control. Nat. Struct. Mol. Biol. 23, 7–15. [PubMed: 26733220]

Buschauer R, Matsuo Y, Sugiyama T, Chen YH, Alhusaini N, Sweet T, Ikeuchi K, Cheng J, Matsuki Y, Nobuta R, et al. (2020). The Ccr4-Not complex monitors the translating ribosome for codon optimality. Science 368, eaay6912.

Chandrasekaran V, Juszkiewicz S, Choi J, Puglisi JD, Brown A, Shao S, Ramakrishnan V, and Hegde RS (2019). Mechanism of ribosome stalling during translation of a poly(A) tail. Nat. Struct. Mol. Biol. 26, 1132–1140. [PubMed: 31768042]

D'Orazio KN, and Green R (2021). Ribosome states signal RNA quality control. Mol. Cell 81, 1372–1383. [PubMed: 33713598]

D'Orazio KN, Wu CC, Sinha N, Loll-Krippleber R, Brown GW, and Green R (2019). The endonuclease Cue2 cleaves mRNAs at stalled ribosomes during No Go Decay. eLife 8, e49117. [PubMed: 31219035]

Daugeron MC, Prouteau M, Lacroute F, and Sé raphin B. (2011). The highly conserved eukaryotic DRG factors are required for efficient translation in a manner redundant with the putative RNA helicase Slh1. Nucleic Acids Res. 39, 2221–2233. [PubMed: 21076151]

Davis AR, Gohara DW, and Yap MN (2014). Sequence selectivity of macrolide-induced translational attenuation. Proc. Natl. Acad. Sci. USA 111, 15379–15384. [PubMed: 25313041]

Decourty L, Saveanu C, Zemam K, Hantraye F, Frachon E, Rousselle JC, Fromont-Racine M, and Jacquier A (2008). Linking functionally related genes by sensitive and quantitative characterization of genetic interaction profiles. Proc. Natl. Acad. Sci. USA 105, 5821–5826. [PubMed: 18408161]

Dimitrova LN, Kuroha K, Tatematsu T, and Inada T (2009). Nascent peptide-dependent translation arrest leads to Not4p-mediated protein degradation by the proteasome. J. Biol. Chem. 284, 10343–10352. [PubMed: 19204001]

Dobin A, Davis CA, Schlesinger F, Drenkow J, Zaleski C, Jha S, Batut P, Chaisson M, and Gingeras TR (2013). STAR: ultrafast universal RNA-seq aligner. Bioinformatics 29, 15–21. [PubMed: 23104886]

Doma MK, and Parker R (2006). Endonucleolytic cleavage of eukaryotic mRNAs with stalls in translation elongation. Nature 440, 561–564. [PubMed: 16554824]

Emsley P, Lohkamp B, Scott WG, and Cowtan K (2010). Features and development of Coot. Acta Crystallogr. D Biol. Crystallogr. 66, 486–501.

Ewels P, Magnusson M, Lundin S, and Käller M. (2016). MultiQC: summarize analysis results for multiple tools and samples in a single report. Bioinformatics 32, 3047–3048. [PubMed: 27312411]

Francis SM, Gas ME, Daugeron MC, Bravo J, and Séraphin B. (2012). Rbg1-Tma46 dimer structure reveals new functional domains and their role in polysome recruitment. Nucleic Acids Res. 40, 11100–11114. [PubMed: 23002146]

Grollman AP (1967). Inhibitors of protein biosynthesis. II. Mode of action of anisomycin. J. Biol. Chem. 242, 3226–3233. [PubMed: 6027796]

Gutierrez E, Shin BS, Woolstenhulme CJ, Kim JR, Saini P, Buskirk AR, and Dever TE (2013). eIF5A promotes translation of polyproline motifs. Mol. Cell 51, 35–45. [PubMed: 23727016]

Guydosh NR, and Green R (2014). Dom34 rescues ribosomes in 3′ untranslated regions. Cell 156, 950–962. [PubMed: 24581494]

Huang W, Sherman BT, and Lempicki RA (2009). Bioinformatics enrichment tools: paths toward the comprehensive functional analysis of large gene lists. Nucleic Acids Res. 37, 1–13. [PubMed: 19033363]

Hannon GJ (2010). FASTX-Toolkit, http://hannonlab.cshl.edu/fastx_toolkit.

Ikeuchi K, Tesina P, Matsuo Y, Sugiyama T, Cheng J, Saeki Y, Tanaka K, Becker T, Beckmann R, and Inada T (2019). Collided ribosomes form a unique structural interface to induce Hel2-driven quality control pathways. EMBO J. 38, e100276.

Ishikawa K, Azuma S, Ikawa S, Semba K, and Inoue J (2005). Identification of DRG family regulatory proteins (DFRPs): specific regulation of DRG1 and DRG2. Genes Cells 10, 139–150. [PubMed: 15676025]

Joazeiro CAP (2019). Mechanisms and functions of ribosome-associated protein quality control. Nat. Rev. Mol. Cell Biol. 20, 368–383. [PubMed: 30940912]

Juszkiewicz S, and Hegde RS (2017). Initiation of Quality Control during Poly(A) Translation Requires Site-Specific Ribosome Ubiquitination. Mol. Cell 65, 743–750.e4. [PubMed: 28065601]

Kumar S, Tomooka Y, and Noda M (1992). Identification of a set of genes with developmentally down-regulated expression in the mouse brain. Biochem. Biophys. Res. Commun. 185, 1155–1161. [PubMed: 1378265]

Kuroha K, Akamatsu M, Dimitrova L, Ito T, Kato Y, Shirahige K, and Inada T (2010). Receptor for activated C kinase 1 stimulates nascent polypeptide-dependent translation arrest. EMBO Rep. 11, 956–961. [PubMed: 21072063]

Labbadia J, and Morimoto RI (2015). The biology of proteostasis in aging and disease. Annu. Rev. Biochem. 84, 435–464. [PubMed: 25784053]

Langmead B, and Salzberg SL (2012). Fast gapped-read alignment with Bowtie 2. Nat. Methods 9, 357–359. [PubMed: 22388286]

Langmead B, Trapnell C, Pop M, and Salzberg SL (2009). Ultrafast and memory-efficient alignment of short DNA sequences to the human genome. Genome Biol. 10, R25. [PubMed: 19261174]

Leipe DD, Wolf YI, Koonin EV, and Aravind L (2002). Classification and evolution of P-loop GTPases and related ATPases. J. Mol. Biol. 317, 41–72. [PubMed: 11916378]

Letzring DP, Dean KM, and Grayhack EJ (2010). Control of translation efficiency in yeast by codon-anticodon interactions. RNA 16, 2516–2528. [PubMed: 20971810]

Li B, and Trueb B (2000). DRG represents a family of two closely related GTP-binding proteins. Biochim. Biophys. Acta 1491, 196–204. [PubMed: 10760581]

Liebschner D, Afonine PV, Baker ML, Bunkóczi G, Chen VB, Croll TI, Hintze B, Hung LW, Jain S, McCoy AJ, et al. (2019). Macromolecular structure determination using X-rays, neutrons and electrons: recent developments in Phenix. Acta Crystallogr. D Struct. Biol. 75, 861–877. [PubMed: 31588918]

Longtine MS, McKenzie A III, Demarini DJ, Shah NG, Wach A, Brachat A, Philippsen P, and Pringle JR (1998). Additional modules for versatile and economical PCR-based gene deletion and modification in Saccharomyces cerevisiae. Yeast 14, 953–961. [PubMed: 9717241]

Love MI, Huber W, and Anders S (2014). Moderated estimation of fold change and dispersion for RNA-seq data with DESeq2. Genome Biol. 15, 550. [PubMed: 25516281]

Lu L, Lv Y, Dong J, Hu S, and Peng R (2016). DRG1 is a potential oncogene in lung adenocarcinoma and promotes tumor progression via spindle checkpoint signaling regulation. Oncotarget 7, 72795–72806. [PubMed: 27626498]

Mahajan MA, Park ST, and Sun XH (1996). Association of a novel GTP binding protein, DRG, with TAL oncogenic proteins. Oncogene 12, 2343–2350. [PubMed: 8649774]

Martin M (2011). Cutadapt removes adapter sequences from highthroughput sequencing reads. EMBnet J. 17, 10–12.

Matsuo Y, Ikeuchi K, Saeki Y, Iwasaki S, Schmidt C, Udagawa T, Sato F, Tsuchiya H, Becker T, Tanaka K, et al. (2017). Ubiquitination of stalled ribosome triggers ribosome-associated quality control. Nat. Commun. 8, 159. [PubMed: 28757607]

Melnikov S, Mailliot J, Shin B-S, Rigger L, Yusupova G, Micura R, Dever TE, and Yusupov M (2016). Crystal Structure of Hypusine-Containing Translation Factor eIF5A Bound to a Rotated Eukaryotic Ribosome. J. Mol. Biol. 428, 3570–3576. [PubMed: 27196944]

Nishimura K, and Kanemaki MT (2014). Rapid Depletion of Budding Yeast Proteins via the Fusion of an Auxin-Inducible Degron (AID). Curr. Protoc. Cell Biol. 64, 20.9.1–20.9.16.

Nersisyan L, Ropat M, and Pelechano V (2020). Improved computational analysis of ribosome dynamics from 5'P degradome data using fivepseq.NAR Genom. Bioinform. 2, lqaa099.

O'Connell A, Robin G, Kobe B, and Botella JR (2009). Biochemical characterization of Arabidopsis developmentally regulated G-proteins (DRGs). Protein Expr. Purif. 67, 88–95. [PubMed: 19460440]

Pelechano V, and Alepuz P (2017). eIF5A facilitates translation termination globally and promotes the elongation of many non polyproline-specific tripeptide sequences. Nucleic Acids Res. 45, 7326–7338. [PubMed: 28549188]

Pelechano V, Wei W, and Steinmetz LM (2015). Widespread Co-translational RNA Decay Reveals Ribosome Dynamics. Cell 161, 1400–1412. [PubMed: 26046441]

Pelechano V, Wei W, and Steinmetz LM (2016). Genome-wide quantification of 5′-phosphorylated mRNA degradation intermediates for analysis of ribosome dynamics. Nat. Protoc. 11, 359–376. [PubMed: 26820793]

Pettersen EF, Goddard TD, Huang CC, Couch GS, Greenblatt DM, Meng EC, and Ferrin TE (2004). UCSF Chimera—a visualization system for exploratory research and analysis. J. Comput. Chem. 25, 1605–1612. [PubMed: 15264254]

Pochopien AA, Beckert B, Kasvandik S, Berninghausen O, Beckmann R, Tenson T, and Wilson DN (2021). Structure of Gcn1 bound to stalled and colliding 80S ribosomes. Proc. Natl. Acad. Sci. USA 118, e2022756118.

Quinlan AR, and Hall IM (2010). BEDTools: a flexible suite of utilities for comparing genomic features. Bioinformatics 26, 841–842. [PubMed: 20110278]

Ranjan N, Pochopien AA, Chih-Chien Wu C, Beckert B, Blanchet S, Green R, V Rodnina M, and Wilson DN (2021). Yeast translation elongation factor eEF3 promotes late stages of tRNA translocation. EMBO J. 40, e106449.

Rohou A, and Grigorieff N (2015). CTFFIND4: Fast and accurate defocus estimation from electron micrographs. J. Struct. Biol. 192, 216–221. [PubMed: 26278980]

Sazuka T, Kinoshita M, Tomooka Y, Ikawa Y, Noda M, and Kumar S (1992a). Expression of DRG during murine embryonic development. Biochem. Biophys. Res. Commun. 189, 371–377. [PubMed: 1280421]

Sazuka T, Tomooka Y, Ikawa Y, Noda M, and Kumar S (1992b). DRG: a novel developmentally regulated GTP-binding protein. Biochem. Biophys. Res. Commun. 189, 363–370. [PubMed: 1449490]

Schellhaus AK, Moreno-Andrés D., Chugh M., Yokoyama H., Moschopoulou A., De S., Bono F., Hipp K., Schäffer E., and Antonin W. (2017). Developmentally Regulated GTP binding protein 1 (DRG1) controls microtubule dynamics. Sci. Rep. 7, 9996. [PubMed: 28855639]

Schenker T, Lach C, Kessler B, Calderara S, and Trueb B (1994). A novel GTP-binding protein which is selectively repressed in SV40 transformed fibroblasts. J. Biol. Chem. 269, 25447–25453. [PubMed: 7929244]

Scheres SH, and Chen S (2012). Prevention of overfitting in cryo-EM structure determination. Nat. Methods 9, 853–854. [PubMed: 22842542]

Schmidt C, Becker T, Heuer A, Braunger K, Shanmuganathan V, Pech M, Berninghausen O, Wilson DN, and Beckmann R (2016a). Structure of the hypusinylated eukaryotic translation factor eIF-5A bound to the ribosome. Nucleic Acids Res. 44, 1944–1951. [PubMed: 26715760]

Schmidt C, Kowalinski E, Shanmuganathan V, Defenouillè re Q., Braunger K., Heuer A., Pech M., Namane A., Berninghausen O., Fromont-Racine M., et al. (2016b). The cryo-EM structure of a ribosome-Ski2-Ski3-Ski8 helicase complex. Science 354, 1431–1433. [PubMed: 27980209]

Schrodinger LLC (2015). The PyMOL Molecular Graphics System, Version 1.8 (Schrodinger, LLC).

Schuller AP, Wu CC, Dever TE, Buskirk AR, and Green R (2017). eIF5A Functions Globally in Translation Elongation and Termination. Mol. Cell 66, 194–205.e5. [PubMed: 28392174]

Shao S, Murray J, Brown A, Taunton J, Ramakrishnan V, and Hegde RS (2016). Decoding Mammalian Ribosome-mRNA States by Translational GTPase Complexes. Cell 167, 1229–1240.e15. [PubMed: 27863242]

Sitron CS, Park JH, and Brandman O (2017). Asc1, Hel2, and Slh1 couple translation arrest to nascent chain degradation. RNA 23, 798–810. [PubMed: 28223409]

Smith T, Heger A, and Sudbery I (2017). UMI-tools: modeling sequencing errors in Unique Molecular Identifiers to improve quantification accuracy. Genome Res. 27, 491–499. [PubMed: 28100584]

Song H, Kim S-I, Ko MS, Kim HJ, Heo JC, Lee HJ, Lee HS, Han IS, Kwack K, and Park JW (2004). Overexpression of DRG2 increases G2/M phase cells and decreases sensitivity to nocodazole-induced apoptosis. J. Biochem. 135, 331–335. [PubMed: 15113831]

Sugiyama T, Li S, Kato M, Ikeuchi K, Ichimura A, Matsuo Y, and Inada T (2019). Sequential Ubiquitination of Ribosomal Protein uS3 Triggers the Degradation of Non-functional 18S rRNA. Cell Rep. 26, 3400–3415.e7. [PubMed: 30893611]

Vazquez-Laslop N, Thum C, and Mankin AS (2008). Molecular mechanism of drug-dependent ribosome stalling. Mol. Cell 30, 190–202. [PubMed: 18439898]

Waterhouse A, Bertoni M, Bienert S, Studer G, Tauriello G, Gumienny R, Heer FT, de Beer TAP, Rempfer C, Bordoli L, et al. (2018). SWISS-MODEL: homology modelling of protein structures and complexes. Nucleic Acids Res. 46, W296–W303. [PubMed: 29788355]

Wickham H, et al. (2011). ggplot2. Wiley Interdiscip. Rev. Comput. Stat. 3, 180–185.

Williams CJ, Headd JJ, Moriarty NW, Prisant MG, Videau LL, Deis LN, Verma V, Keedy DA, Hintze BJ, Chen VB, et al. (2018). MolProbity:More and better reference data for improved all-atom structure validation. Protein Sci. 27, 293–315. [PubMed: 29067766]

Wilson DN, and Beckmann R (2011). The ribosomal tunnel as a functional environment for nascent polypeptide folding and translational stalling. Curr. Opin. Struct. Biol. 21, 274–282. [PubMed: 21316217]

Wolff S, Weissman JS, and Dillin A (2014). Differential scales of protein quality control. Cell 157, 52–64. [PubMed: 24679526]

Wout PK, Sattlegger E, Sullivan SM, and Maddock JR (2009). Saccharomyces cerevisiae Rbg1 protein and its binding partner Gir2 interact on Polyribosomes with Gcn1. Eukaryot. Cell 8, 1061–1071. [PubMed: 19448108]

Xu X, Lambrecht AD, and Xiao W (2014). Yeast survival and growth assays. Methods Mol. Biol. 1163, 183–191. [PubMed: 24841307]

Yan LL, Simms CL, McLoughlin F, Vierstra RD, and Zaher HS (2019). Oxidation and alkylation stresses activate ribosome-quality control. Nat. Commun. 10, 5611. [PubMed: 31819057]

Zeng F, and Jin H (2016). Peptide release promoted by methylated RF2 and ArfA in nonstop translation is achieved by an induced-fit mechanism. RNA 22, 49–60. [PubMed: 26554029]

Zeng F, Chen Y, Remis J, Shekhar M, Phillips JC, Tajkhorshid E, and Jin H (2017). Structural basis of co-translational quality control by ArfA and RF2 bound to ribosome. Nature 541, 554–557. [PubMed: 28077875]

Zhao X-F, and Aplan PD (1998). SCL binds the human homologue of DRG in vivo. Biochim. Biophys. Acta 1448, 109–114. [PubMed: 9824680]

Zheng SQ, Palovcak E, Armache JP, Verba KA, Cheng Y, and Agard DA (2017). MotionCor2: anisotropic correction of beam-induced motion for improved cryo-electron microscopy. Nat. Methods 14, 331–332. [PubMed: 28250466]

Zivanov J, Nakane T, Forsberg BO, Kimanius D, Hagen WJ, Lindahl E, and Scheres SH (2018). New tools for automated high-resolution cryo-EM structure determination in RELION-3. eLife 7, e42166. [PubMed: 30412051]

Highlights

- Rbg1/Tma46 works at the junction of protein synthesis and quality control
- Rbg1/Tma46 promotes translational initiation, elongation, and termination
- Rbg1's G domain binds to the ribosome using a different conformation than other trGTPases
- Tma46's zinc finger binds to the gap between 40S head and shoulder in the paused ribosome

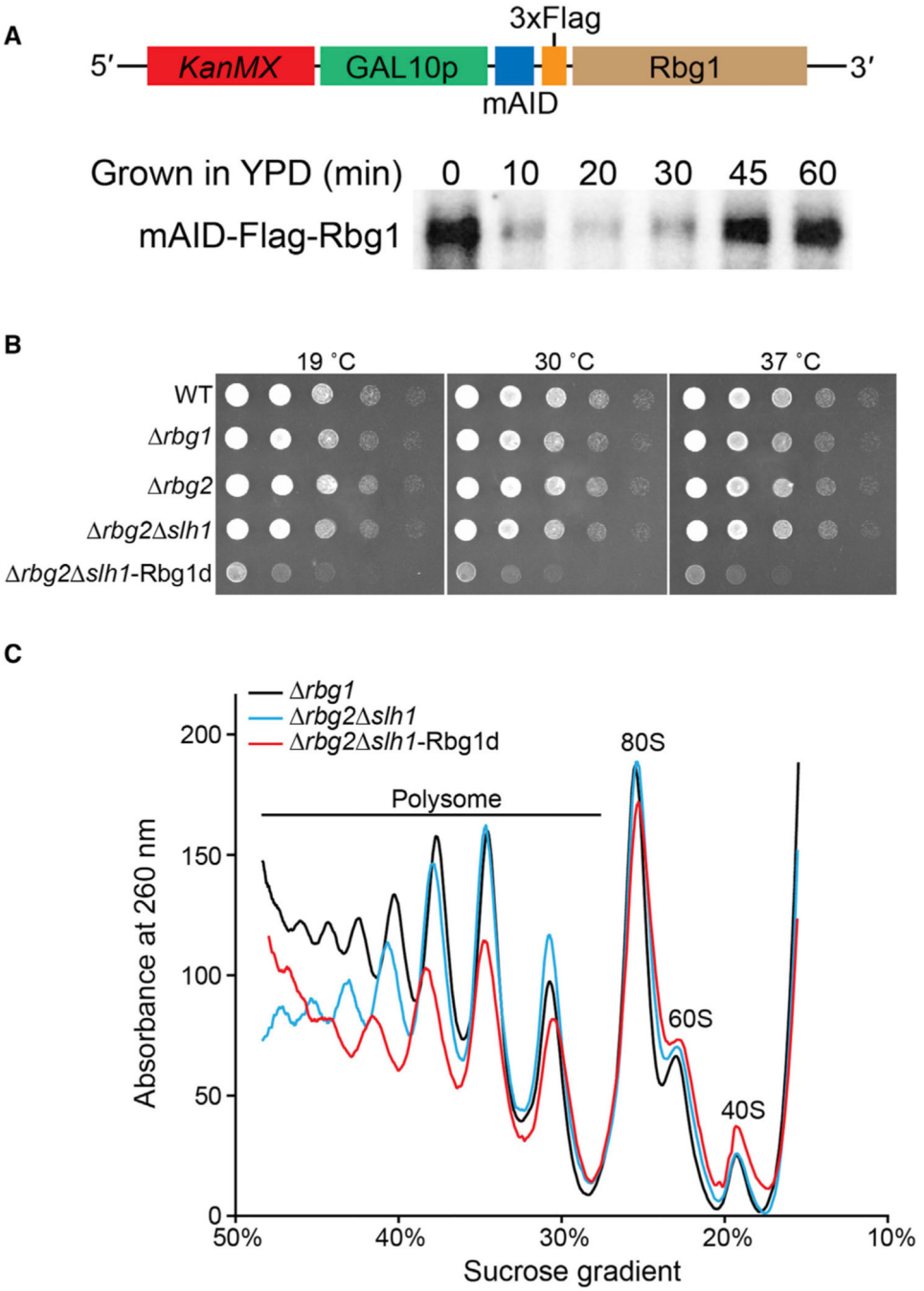

Figure 1. Rbg proteins play important roles in global translation

(A) Model of the auxin-inducible-degron system.To remove the Rbg1 protein from the cell, a GAL10 promoter was inserted into the 5′ UTR of the *rbg1* gene so that Rbg1 transcription levels can be controlled by the presence of glucose in the media. A mini auxin-inducible degron (mAID) tag was fused to the N terminus of Rbg1. Cells were first grown in YPGR medium and then changed to YEPD medium containing 1 mM auxin to induce the degradation of the Rbg1 protein in the cell. Aliquots at different time points were acquired, and the Rbg1 protein levels were monitored by western blot with an anti-FLAG antibody.

With the mAID degron tag, the Rbg1 protein degrades after 20 min, but its expression is restored after 45 min. The western blot represents one of three biological replicates.

(B) Elimination of Rbg1 under Δ*rbg2*Δ*slh1* background shows a temperature-independent growth defect. Serial dilutions of liquid cultures growing in exponential phase were spotted on YEPD plates containing 1 mM auxin and were incubated for 2 days at 30°C or 37°C or for 4 days at 19°C.

(C) Polysome profiles from cells incubated for20 min in YEPD indicate that Rbg1 plays an important role in global translation. Cells were first grown in YPGR medium to an optical density 600 (OD_{600}) of 0.6 and then were changed to YEPD medium containing 1 mM auxin for 20 min. Cells were then quickly harvested and polysome profiling was performed. The profiles of wild-type (WT) and Δ*rbg2* strains are not shown here because WT, Δ*rbg2*, and Δ*rbg1* have nearly identical profiles. These data represent one of three biological replicates.

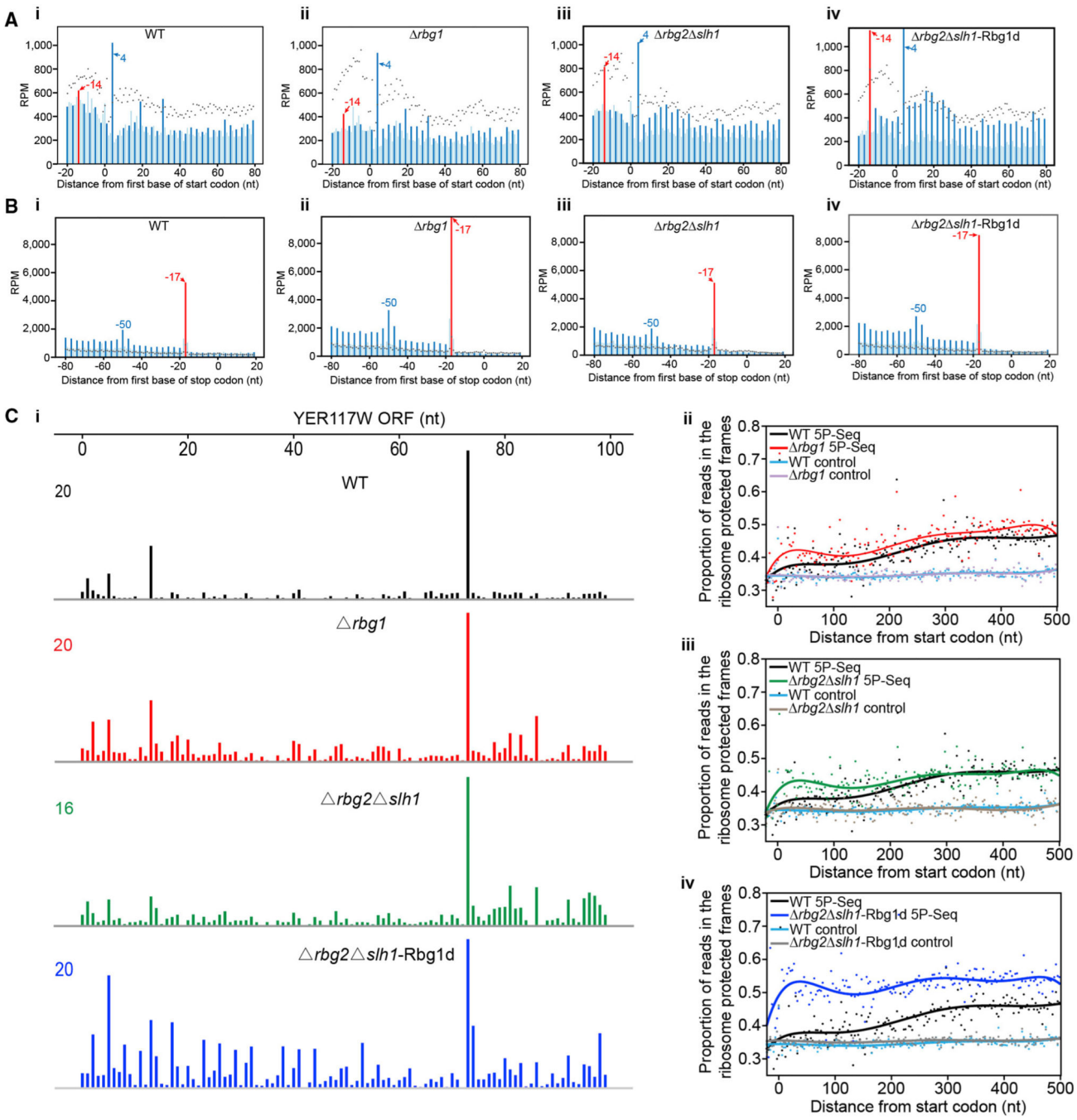

Figure 2. Deletion of Rbg1 results in slow translation initiation, elongation, and termination

(A) Translation initiation arrests in mutant cells. Normal translation pauses at start codons in WT cells; and increased ribosome pauses at start codons in Δ*rbg1*, Δ*rbg2*Δ*slh1*, and Δ*rbg2*Δ*slh1*-Rbg1d cells. Metagene analysis displays the abundance of 5′P reads relative to start codons for WT, Δ*rbg1*, Δ*rbg2*Δ*slh1*, and Δ*rbg2*Δ*slh1*-Rbg1d strains or after random fragmentation (5P-Seq control, dotted black line). Reads are represented by rpm, with the blue bar indicating the +1 frame and light blue bars indicating the 0 and +2 frames. The red peak at −14 nt corresponds to the protected region from a putative initiation-

paused ribosome, and the blue peak at 4 nt is caused by peptide-induced ribosomal arrest. Biological replicates are averaged.

(B) Effects on translation termination in mutant cells. Normal translation pauses at stop codons in WT cells and altered pauses in the three mutants Δ*rbg1*, Δ*rbg2*Δ*slh1*, and Δ*rbg2*Δ*slh1*-Rbg1d. Red peaks at the −17-nt position denote ribosomes with a stop codon in the A-site; and the pause at the −50-nt position is indicative of a disome position, with the leading ribosome reaching translation termination. Other experimental details are the same as described in (A). (C) Slower translational elongation after depletion of Rbg1, Rbg2, and Slh1. i. Representative genome tracks of the 5′ ends of 5P-Seq reads in WT (black), Δ*rbg1* (red), Δ*rbg2*Δ*slh1* (green), and Δ*rbg2*Δ*slh1*-Rbg1d strains (blue). Coverage is expressed in rpm. An obvious 3-nt periodicity pattern was observed for YER177W mRNA in the Δ*rbg2*Δ*slh1*-Rbg1d strain. ii–iv. The proportion of 5P-Seq reads in the ribosome-protected frame (frame 1 in Figure S2) shows that the 5′ end of coding regions was protected by ribosomes in the Δ*rbg2*Δ*slh1*-Rbg1d strain. Proportion scores were calculated for each codon by normalizing the read counts in frame 1 to the total reads in all three frames within the same codon. These are shown as dots with smoothed lines (polynomial fitting) for genes longer than 1,000 base pairs (bp) and with reads per million per kilobase (RPKM) values of >20. Only the region containing −20 nt to 501 nt with respect to the first base of start codon was used to calculate the proportion score. 5P-Seq samples from Drbg1 (ii, red), Δ*rbg2*Δ*slh1* (iii, green), and Δ*rbg2*Δ*slh1*-Rbg1d (iv, blue) strains were compared to WT strains (black). Random fragmentation samples (control) are also shown. Biological replicates are averaged.

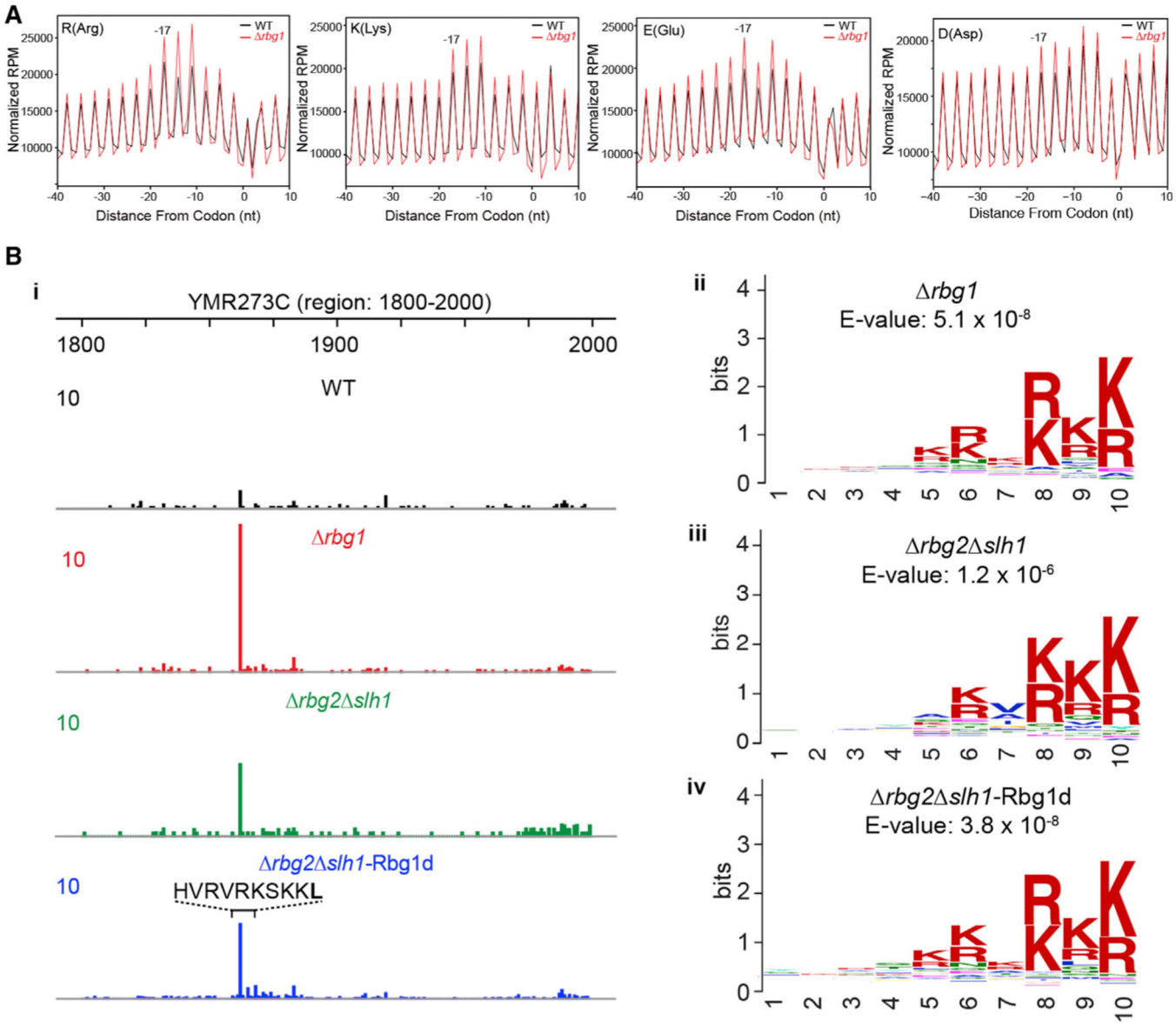

Figure 3. Deletion of Rbg1 results in ribosome pauses at certain amino acids and R/K-rich regions in the mRNA

(A) Increased translation pauses at arginine, lysine, glutamic acid, and aspartic acids positions in the absence of Rbg1. The metagene (−40 to +10 window) shows the number of 5P intermediates from translation of arginine, lysine, glutamic acid, and aspartic acids amino acids and their ribosomal positions in Δ*rbg1* (red lines) and WT (black lines) cells. The total number of reads was normalized to facilitate data analysis and comparison, and data were analyzed as described (Pelechano and Alepuz, 2017). The peaks at −17 nt, −14 nt, and −11 nt represent indicated codons at the ribosomal A-, P-, and E-sites, respectively. The normalized rpms for each amino acid between the WT and Δrbg1 were compared, and the adjusted p values at the −17 position were shown. The adjusted p value was calculated using the Benjamin-Hochberg method in R package called DESeq2 (Love et al., 2014). The

adjusted $p < 0.01$ was used as the criterion for a significantly regulated difference in the data.

(B) Rbg1 alleviates ribosome pausing at arginine/lysine-rich regions. i. Representative genome tracks of 5′ ends of 5P-Seq reads. Genome tracks of the 5′ ends of 5P-Seq reads in WT (black), Δ*rbg*1 (red), Δ*rbg2*Δ*slh1* (green), and Δ*rbg2*Δ*slh1*-Rbg1d (blue) strains were shown around the arginine-/lysine-rich region. Coverage is expressed in average rpm of the biological duplicates. ii–iv. Translation pauses at the R-/K-rich region in Δ*rbg1*, Δ*rbg2*Δ*slh1*, and Δ*rbg2*Δ*slh1*-Rbg1d strains. To identify specific peptide sequences that induce ribosome pausing while being translated in the knockout strains, pause scores were first calculated by dividing the rpm value at each position of the transcript by the mean rpm value for the 10 codons upstream and downstream of the same position. The 10 amino acids upstream with a pause score of >10 were compared to those with pause scores of <10 by using MEME (Bailey et al., 2009). E-values were defined by MEME. Amino acid sequences extracted from the WT strain show no consensus sequence.

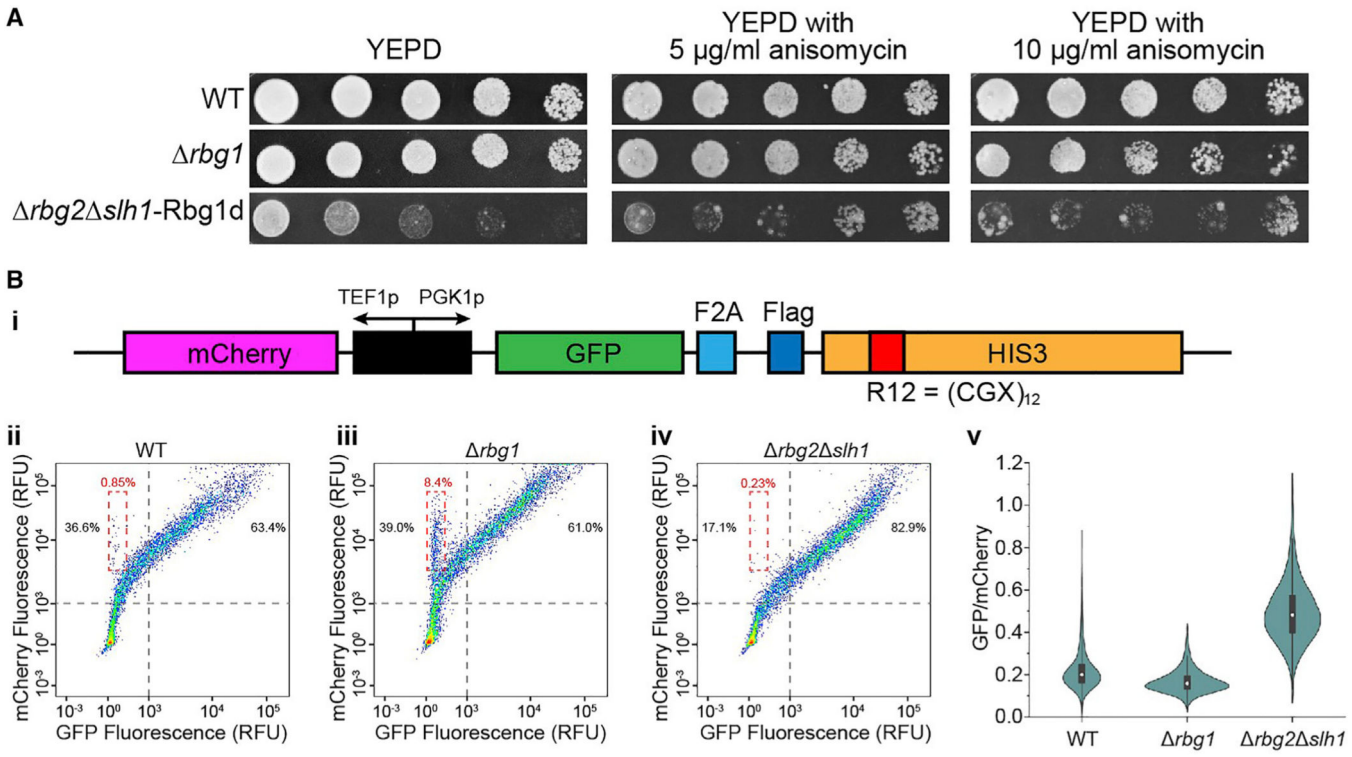

Figure 4. Rbg1 suppresses ribosome pauses and promotes efficient translation

(A) Deletion of Rbg1 results in the slower growth of yeast cells in the presence of anisomycin. Serial dilutions of liquid cultures growing in exponential phase were spotted on YEPD, in the absence or presence of different concentrations of anisomycin. Cells were incubated at 30°C, and pictures were taken after 2 days (without anisomycin) or 3 days (with anisomycin).

(B) Rbg1 enhances translation of mRNAs harboring an intrinsic stalling sequence. Yeast cells expressing the indicated mRNA with the R12 sequence, fluorescent mCherry, and GFP reporters (top panel) were grown to exponential phase (OD_{600}, 0.6) and were analyzed by flow cytometry. mCherry and GFP fluorescence intensities in the cell were monitored simultaneously by using 561-nm and 488-nm excitation lasers, respectively. Scatterplots of 10,000 individual cells of the WT, Δ*rbg1*, and Δ*rbg2*Δ*slh1* background are displayed separately. The scatterplots are shown on a bi-exponential scale with pseudo-color in order to better visualize data across the wide range of expression levels seen in these experiments. According to the control cells that do not express the indicated mRNA construct (data not shown), only the cells with more than 10^3 relative fluorescence unit (RFU) of mCherry fluorescence are considered to contain enough mRNAs and are subjected to further analysis. WT, Δ*rbg1*, and Δ*rbg2*Δ*slh1* cells with $>10^3$ RFU mCherry intensities are divided into two groups and shown as percentages in gray dashed lines. Cells in the dashed box have high mCherry expression levels but low GFP expression levels, the amount of which in WT, Δ*bg1*, and Δ*rbg2*Δ*slh1* is shown accordingly as percentages (red) (ii, iii, and iv). The relative cell quantities at each position are indicated using a red-to-blue spectrum, for which the red color represents the largest cell population and blue represents the smallest one. v. Normalized reporter GFP levels. For WT, Δ*rbg1*, and Δ*rbg2*Δ*slh1* cells with $>10^3$ RFU

mCherry intensities, the GFP intensity is normalized to the corresponding mCherry intensity. The ratio of GFP/mCherry intensities obtained from flow cytometry data in WT, Δ*rbg1*, and Δ*rbg2*Δ*slh1* are compared using violin plots (center dots, median; boxes, 25th to 75th percentiles; whiskers, 1.5× interquartile range [IQR]). Median values for the GFP/mCherry ratios in WT, Δ*rbg1*, and Δ*rbg2*Δ*slh1* are 0.200, 0.158, and 0.482, respectively.

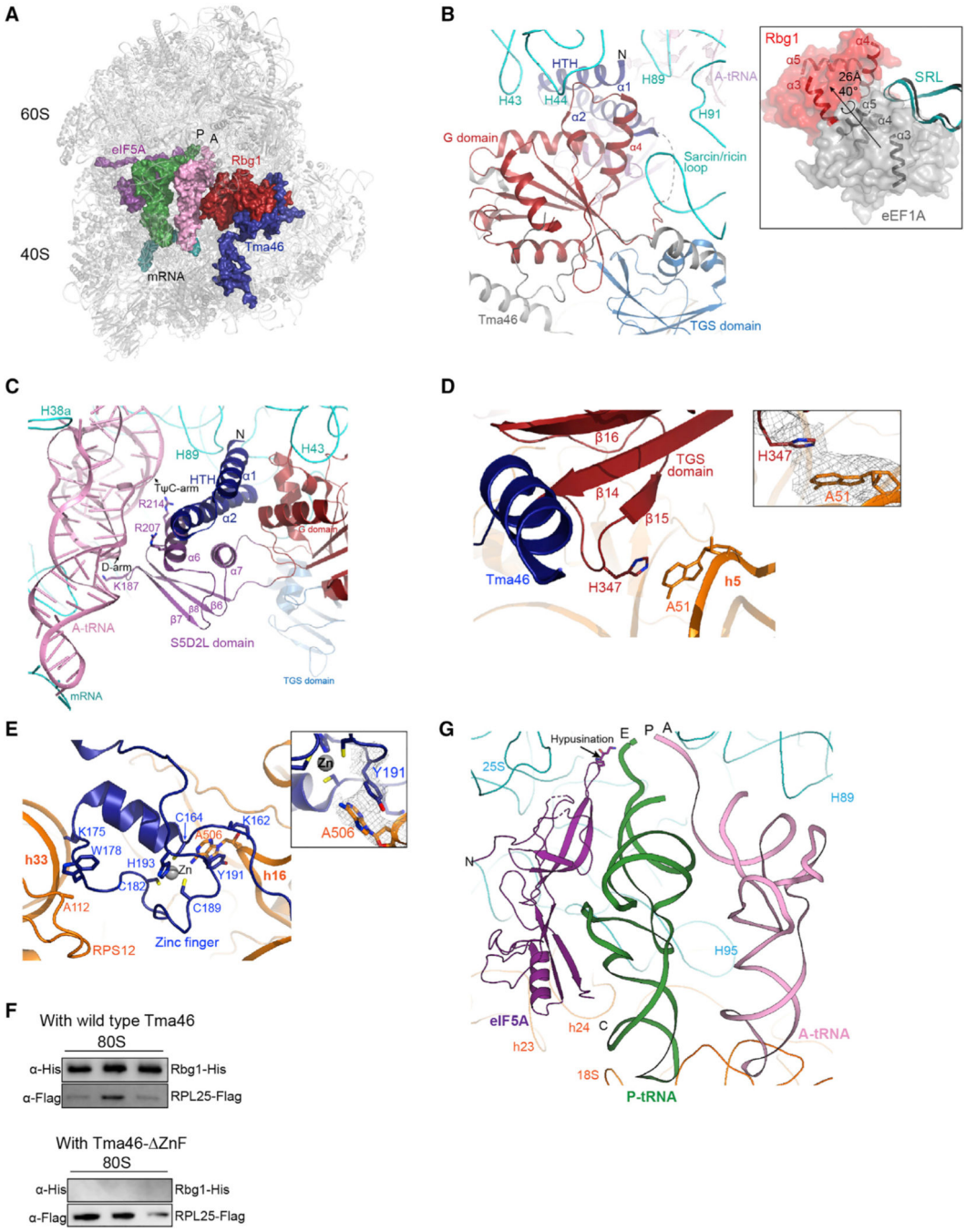

Figure 5. Structural basis for enhanced translation when Rbg1/Tam46 binds to a paused ribosome

(A) An overall structure of Rbg1/Tma46-bound ribosomes. The ribosome is colored in gray. P-tRNAs, A-tRNAs-nascent peptides, eIF5A, Rbg1, and Tma46 are colored in green, pink, magenta, red, and blue, respectively.

(B–E) Detailed essential interactions of the Rbg1 G domain with the sarcin-ricin loop (B), S5D2L domain with A-tRNA (C), TGS domain with h5 in the 40S subunit (D), and the second zinc finger in Tma46 with the head and shoulder regions of the 40S subunit (E) are shown. The insert in (B) shows conformational changes in the G domain of Rbg1 in

this study (red surface) and eEF1A (gray surface, with GDP and Didemnin B bound, PDB: 5LZS; Shao et al., 2016) on the ribosome when the 25S rRNAs are aligned. Helices α3–α5 are shown in Rbg1 and eEF1A to illustrate conformational changes of the G domain in the ribosome.

(F) The Rbg1/Tma46 complex binds to the ribosome by the zinc-finger domain of Tma46. Proteins co-expressed in the *Escherichia coli* BL21 strain were purified and incubated with pure 80S ribosomes, and then ribosomal complexes were separated by sedimentation through a 10%–50% sucrose gradient. Binding of Rbg1/Tma46 to the ribosome was determined by western blot. FLAG-tagged RPL25 was immunoblotted on the same membrane. Both the GTP- and GDP-bound heterodimeric GTPases bound to the 80S ribosome, but only the GTP-bound state is shown. The western blot represents one of three biological replicates.

(G) Conformation of eIF5A in the Rbg1/Tma46-bound ribosomes. eIF5A binds to the E-site in the Rbg1/Tma46-bound ribosomal complex. eIF5A (purple), P-tRNA (green), and A-tRNA (pink) are represented as cartoons. The site of hypusination in eIF5A can be determined according to the density in the complex. Ribosome proteins are removed for clarity, and 25S rRNA (cyan) and 18S rRNA (orange) are shown.

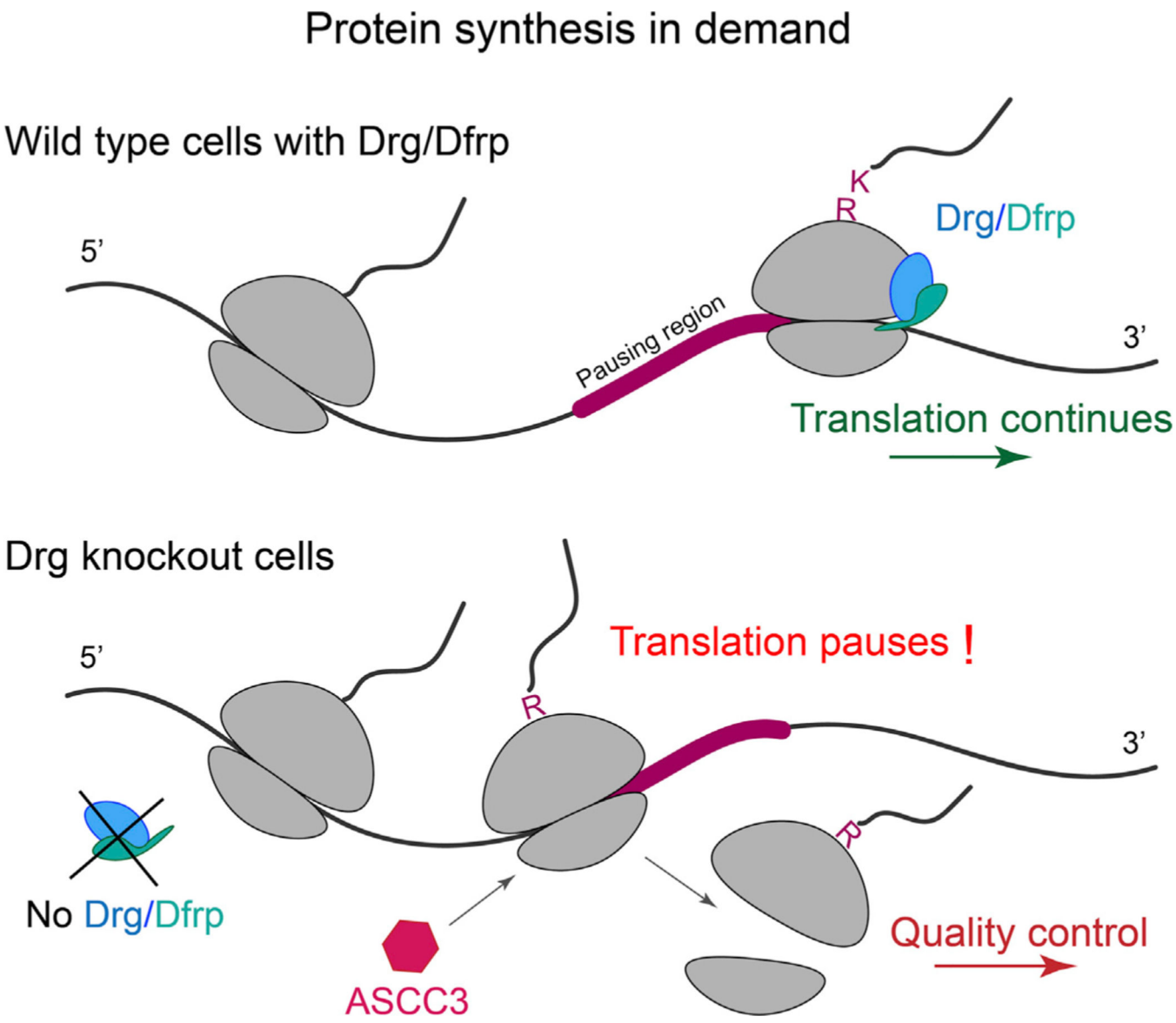

Figure 6. Functional interplay of Drg/Dfrp and ASCC3 in the translation pause-and-resume and quality-control pathways

When translation pauses, Drg/Dfrp senses the paused ribosome, stabilizes ribosomes in the productive conformation, and promotes efficient translation, thereby allowing ribosomes to continue translating the mRNA. In the absence of Drg/Dfrp, another protein called ASCC3 binds the stalled ribosome and triggers RQC involving ribosome subunit disassociation, mRNA degradation, and no-go decay.

KEY RESOURCES TABLE

REAGENT or RESOURCE	SOURCE	IDENTIFIER
Antibodies		
Monoclonal ANTI-FLAG® M2 antibody	Sigma-Aldrich	Cat# F3165; RRID:AB_259529
Monoclonal Anti-polyHistidine antibody produced in mouse	Sigma-Aldrich	Cat# H1029; RRID:AB_260015
Bacterial and virus strains		
E. coli: BL21(DE3)	Agilent Technologies	Cat# 230134
Chemicals, peptides, and recombinant proteins		
β,γ-Methyleneguanosine 5′-triphosphate sodium salt (GDPCP)	Sigma-Aldrich	Cat# M3509-25MG
Anisomycin	Sigma-Aldrich	Cat# A5862-0.5ML
Cycloheximide	Sigma-Aldrich	Cat# C7698–1G
Protease Inhibitor Cocktail Tablets in EASYpacks (ROCHE)	Sigma-Aldrich	Cat# 4693159001
SUPERase · In RNase Inhibitor (20U/μL)	Fisher Scientific	Cat# AM2696
T4 Polynucleotide Kinase	NEB	Cat# M0201S
Dynabeads® mRNA DIRECT Purification Kit	Invitrogen	Cat# 61011
Phusion® High-Fidelity PCR Master Mix with HF Buffer	NEB	Cat# M0531S
Dynabeads® M-280 Streptavidin	Invitrogen	Cat# 11205D
HighPrep PCR Clean-up System	Magbio	Cat# AC-60005
SuperScript II Reverse Transcriptase	Thermo Fisher	Cat# 18064022
Auxin	Sigma	Cat# I2886-25G
TURBO DNase	Invitrogen	Cat# AM2238
T4 RNA ligase	Promega	Cat# M1051
n-dodecyl-D-maltoside (DDM)	Macklin	CAS# 69227-93-6
Glutaraldehyde	Sagon	Cat# A500484-0250
Quantifoil grids 300mesh 1.2/1.3 copper	Quantifoil	Cat# BQR1.2/1.3-3C
IgG beads	Smart-lifesciences	Cat# SA082010
Critical commercial assays		
Q5® Site-Directed Mutagenesis Kit	NEB	Cat# E0552S
Deposited data		
Rabbit 80S ribosome stalled on a poly(A) tail	Chandrasekaran et al., 2019	PDB: 6SGC
Crystal structure of Rbg1/Tma46 complex	Francis et al., 2012	PDB: 4A9A
The structure of the eukaryotic ribosome	Ben-Shem et al., 2011	PDB: 4V88
Structure of mammalian ribosome with eEF1A	Shao et al., 2016	PDB: 5LZS
Yeast 60S ribosomal subunit with A-site tRNA, P-site tRNA and eIF-5A	Schmidt et al., 2016a	PDB: 5GAK
Yeast 80S ribosome bound to eEF3 and A/A- and P/P-tRNAs	Ranjan et al., 2021	PDB: 7B7D

REAGENT or RESOURCE	SOURCE	IDENTIFIER
5P-sequencing Data	This paper	NCBI Gene Expression Omnibus: GSE154212
Electron Microscopy Maps	This paper	Electron Microscopy Databank: EMD-24652
Rbg1-Tma46 bound 80S Coordinates	This paper	PDB: 7RR5
Seq_compareDuplicate.py	This paper	https://doi.org/10.6084/m9.figshare.16567662
Seq_metageneWheatmap.py	This paper	https://doi.org/10.6084/m9.figshare.16567686
Seq_periodicity.py	This paper	https://doi.org/10.6084/m9.figshare.16567719
Seq_proportion.py	This paper	https://doi.org/10.6084/m9.figshare.16567728
Seq_stalling.py	This paper	https://doi.org/10.6084/m9.figshare.16567734
Experimental models: Organisms/strains		
S. *cerevisiae*: Strain Background: BY4742, see Table S1	Gift from Rutilio Fratti, University of Illinois at Urbana-Champaign	N/A
Oligonucleotides		
rP5_RND	IDT (Pelechano et al., 2016)	No catalog number available for customized order in IDT
BioNotI-P5- PET	IDT (Pelechano et al., 2016)	N/A
P7MPX_linker _for	This paper	N/A
P7MPX_linker _rev	IDT (Pelechano et al., 2016)	N/A
PE1.0	IDT This paper	N/A
PE2_MPX_XX (XX = 01–08)	IDT This paper	N/A
See Table S3 for full list of oligonucleotides used in this study	N/A	N/A
Recombinant DNA		
Plasmid: pGAL10-mAID	This paper	N/A
Plasmid: p415G-TAP-URA3	This paper	N/A
Plasmid: pPGK1	This paper	N/A
Plasmid: pPGK1-Rbg1	This paper	N/A
Plasmid: pET28a-Rbg1	This paper	N/A
Plasmid: pET22b-Tma46	This paper	N/A
Plasmid: pET22b-Tma46ΔZnF	This paper	N/A
Software and algorithms		
Cutadapt	Martin, 2011	RRID: SCR_011841, https://cutadapt.readthedocs.io/en/stable/
Bbmap	Joint Genome Institute	RRID:SCR_016965, https://sourceforge.net/projects/bbmap/
fastx_trimmer (FASTX-Toolkit)	Hannon, 2010	RRID: SCR_005534, http://hannonlab.cshl.edu/fastx_toolkit/
Bowtie1	Langmead et al., 2009	RRID: SCR_005476, http://bowtie-bio.sourceforge.net/index.shtml
Bowtie2	Langmead and Salzberg, 2012	RRID: SCR_016368, http://bowtie-bio.sourceforge.net/index.shtml
UMI-tools	Smith et al., 2017	RRID:SCR_017048, https://umi-tools.readthedocs.io/en/latest/

REAGENT or RESOURCE	SOURCE	IDENTIFIER
STAR	Dobin et al., 2013	RRID:SCR_004463, https://github.com/alexdobin/STAR
BEDTools	Quinlan and Hall, 2010	RRID:SCR_006646, https://bedtools.readthedocs.io/en/latest/
FastQC	Babraham Bioinformatics, Babraham Institute	RRID:SCR_014583, https://www.bioinformatics.babraham.ac.uk/projects/fastqc
MultiQC	Ewels et al., 2016	RRID:SCR_014982, https://multiqc.info
Fivepseq	Nersisyan et al., 2020	http://pelechanolab.com/software/fivepseq/
Ggplot2	Wickham et al., 2011	RRID:SCR_014601, https://ggplot2.tidyverse.org
MEME	Bailey et al., 2009	RRID:SCR_001783, https://meme-suite.org/meme/
Flow JO	FlowJo, LLC	https://www.flowjo.com/
Origin	OriginLab Corporation	RRID:SCR_014212, https://www.originlab.com
Relion 3	Zivanov et al., 2018	RRID:SCR_016274, https://www3.mrc-lmb.cam.ac.uk/relion/index.php?title=Main_Page
Chimera	Petterson et al., 2004	RRID:SCR_004097, https://www.cgl.ucsf.edu/chimera/
Pymol	Schrodinger, LLC	RRID:SCR_000305, https://pymol.org/2/
MotionCor2	Zheng et al., 2017	RRID:SCR_016499, https://emcore.ucsf.edu/ucsf-software
CTFFIND4	Rohou and Grigorieff, 2015	RRID:SCR_016732, https://grigoriefflab.umassmed.edu/ctffind4
Coot	Emsley et al., 2010	RRID:SCR_014222, https://www2.mrc-lmb.cam.ac.uk/personal/pemsley/coot/
SWISS-MODEL	Waterhouse et al., 2018	RRID:SCR_018123, https://swissmodel.expasy.org
Phenix	Liebschner et al., 2019	RRID:SCR_014224, https://phenix-online.org
MolProbity	Williams et al., 2018	RRID:SCR_014226, http://molprobity.biochem.duke.edu